



CERN-EP-2023-191
29 August 2023

Probing the Chiral Magnetic Wave with charge-dependent flow measurements in Pb–Pb collisions at the LHC

ALICE Collaboration*

Abstract

The Chiral Magnetic Wave (CMW) phenomenon is essential to provide insights into the strong interaction in QCD, the properties of the quark–gluon plasma, and the topological characteristics of the early universe, offering a deeper understanding of fundamental physics in high-energy collisions. Measurements of the charge-dependent anisotropic flow coefficients are studied in Pb–Pb collisions at center-of-mass energy per nucleon–nucleon collision $\sqrt{s_{\text{NN}}} = 5.02$ TeV to probe the CMW. In particular, the slope of the normalized difference in elliptic (v_2) and triangular (v_3) flow coefficients of positively and negatively charged particles as a function of their event-wise normalized number difference, is reported for inclusive and identified particles. The slope r_3^{Norm} is found to be larger than zero and to have a magnitude similar to r_2^{Norm} , thus pointing to a large background contribution for these measurements. Furthermore, r_2^{Norm} can be described by a blast wave model calculation that incorporates local charge conservation. In addition, using the event shape engineering technique yields a fraction of CMW (f_{CMW}) contribution to this measurement which is compatible with zero. This measurement provides the very first upper limit for f_{CMW} , and in the 10–60% centrality interval it is found to be 26% (38%) at 95% (99.7%) confidence level.

arXiv:2308.16123v2 [nucl-ex] 8 Jan 2024

1 Introduction

The primary goal of relativistic heavy-ion collisions at the Large Hadron Collider (LHC) is to study the properties of the emerging strongly interacting medium called the quark–gluon plasma (QGP) [1–6]. The transition from normal hadronic matter to the QGP is predicted by quantum chromodynamics (QCD) calculations on the lattice [7, 8]. Heavy-ion collisions are also characterized by extremely strong short-lived electromagnetic fields ($B \sim 10^{18}$ Gauss), primarily induced by protons from the incoming nuclei that do not undergo any inelastic collision and are referred to as spectators [9]. The direction of \mathbf{B} is perpendicular to the reaction plane, the plane spanned by the impact parameter of the colliding nuclei and the beam direction. The presence of this intense magnetic field allows for the possibility to study novel QCD phenomena, such as parity violation in strong interactions [10–12].

The potential to observe parity violation in strong interactions using ultrarelativistic heavy-ion collisions was first discussed in Refs. [12–14] and further reviewed in Refs. [15–18]. Theoretically, the interactions of quarks with gluonic fields describing transitions between topologically different QCD vacuum states change the quark chirality, leading to a local chiral imbalance. The strong magnetic field leads to a charge separation (electric current) relative to the reaction plane, which is known as the Chiral Magnetic Effect (CME) [12, 19–24]. The experimental search for the CME using heavy-ion collisions has intensified over the past decade. Though early measurements pointed to some similarities between the results and the theoretical predictions [25–27], there is substantial evidence that background sources, i.e., collective phenomena and local charge conservation (LCC), play a significant role in the experimental measurements [28, 29]. The LCC here refers to the principle that within a local region of a physical system, the balance or conservation of quantum numbers for eg., electric charge is upheld. Experimental results indicate that the upper limit of the CME signal contribution ranges from 7% to 20% at 95% confidence level in semicentral heavy-ion collisions [25–39].

A dual phenomenon to the CME is the Chiral Separation Effect (CSE) [40, 41], which is theorized to induce a chirality current along \mathbf{B} in the presence of a finite electric chemical potential (μ_e). The CME and the CSE interact with one another forming a long wavelength collective excitation, called the Chiral Magnetic Wave (CMW) [42–46]. Similar to the CME-induced electric dipole moment, the CMW would manifest itself in a finite electric quadrupole moment in the final state [42]. This effect, if present, can be measured by charge-dependent anisotropic flow measurements [42]. The anisotropic flow is quantified in terms of the Fourier coefficients v_n of the azimuthal distribution of the produced particles with respect to the n^{th} -order event plane angle Ψ_n [47–49]

$$\frac{dN}{d\varphi} \propto 1 + \sum_{n=1}^{\infty} 2v_n \cos[n(\varphi - \Psi_n)], \quad (1)$$

where φ is the azimuthal angle of a particle. The first three coefficients v_1 , v_2 , and v_3 are known as the directed, elliptic, and triangular flow, respectively. The CMW-induced electric quadrupole moment evolves with the medium expansion, leading to an increase (decrease) of v_2 for negatively (positively) charged hadrons [42]. The difference between negatively and positively charged hadron v_2 (Δv_2) is expected to be proportional to the event-by-event charge asymmetry (A_{ch}) [42, 43],

$$\Delta v_2 = v_2^- - v_2^+ \propto r_2 A_{\text{ch}}. \quad (2)$$

In the above equation, r_2 denotes the slope parameter between Δv_2 and event-by-event charge asymmetry, and A_{ch} is defined as

$$A_{\text{ch}} = \frac{(N^+ - N^-)}{(N^+ + N^-)}, \quad (3)$$

where N^+ (N^-) are positively (negatively) charged hadrons measured in a given event.

The first experimental search for the CMW was performed by the STAR Collaboration at the Relativistic Heavy Ion Collider (RHIC) with charged pions in Au–Au collisions at center-of-mass energy per

nucleon–nucleon collision $\sqrt{s_{\text{NN}}} = 200$ GeV [50], in which a positive linear dependence on A_{ch} was observed for the v_2 difference between π^- and π^+ . The extracted positive slopes as well as their centrality dependence agree well with theoretical calculations [42–44]. A similar positive correlation was measured by the ALICE Collaboration at the Large Hadron Collider (LHC) with charged hadrons in semicentral Pb–Pb collisions at $\sqrt{s_{\text{NN}}} = 2.76$ TeV [51]. Comparable slopes to those from Au–Au collisions in semicentral collisions were reported. However, the lifetime of the magnetic field in vacuum is expected to drop much faster at LHC energies compared to that at RHIC energies [52]. Thus, it is highly unlikely that an identical slope value would be observed by different experiments with orders of magnitude difference in collision energies. Furthermore, a similar linear dependence was observed by the precision measurements of the CMS collaboration in p–Pb and Pb–Pb collisions at $\sqrt{s_{\text{NN}}} = 5.02$ TeV [53]. This similarity questioned the CMW interpretation since the CMW signal is not expected to be present in p–Pb collisions due to the decoupling of the magnetic field from the reaction plane in such collisions [34, 54]. In addition, both STAR and CMS collaborations have observed a linear dependence between A_{ch} and Δv_3 , i.e. the difference between the v_3 coefficients of negatively and positively charged hadrons [53, 55]

$$\Delta v_3 = v_3^- - v_3^+ \propto r_3 A_{\text{ch}}. \quad (4)$$

However, this should not originate from the CMW-induced electric quadrupole configuration in the medium as the CMW is mainly driven by the magnetic field which is uncorrelated with the third order event plane. As a result of these observations, it appears likely that the slope observed in Δv_2 as a function of A_{ch} is not due to the CMW processes only. To ease the comparison between measurements performed by different experiments, one can define a normalized slope parameter as,

$$\Delta v_n^{\text{Norm}} = \frac{v_n^- - v_n^+}{(v_n^- + v_n^+)/2} \propto r_n^{\text{Norm}} A_{\text{ch}}, \quad (5)$$

where $n = 2$ or 3 . Recently, it was proposed in Ref. [56], that one can also utilize the event shape engineering (ESE) technique [57] to estimate the CMW signal. This selection methodology was already employed to constrain the CME [33, 36]. The ESE approach utilizes the fluctuations in the shape of the initial state of the system and allows one to select events with the same centrality but different initial geometry, thus varying the background contributions. Instead of the $A_{\text{ch}}-v_2$ slope, an alternative observable, the integral covariance [51] can be used. It is defined as

$$\Delta \text{IC} = \left(\langle v_2^- A_{\text{ch}} \rangle - \langle A_{\text{ch}} \rangle \langle v_2^- \rangle \right) - \left(\langle v_2^+ A_{\text{ch}} \rangle - \langle A_{\text{ch}} \rangle \langle v_2^+ \rangle \right), \quad (6)$$

where the angular bracket denotes the average over the events. This observable, by definition, calculates the covariance between A_{ch} and v_2 and is equivalent to the slope parameter. The main advantage of such a covariance is the removal of the dependence on the detector acceptance and on the reconstruction efficiency of charged hadrons when expressed differentially [51]. In addition, one no longer needs to divide each sub-sample of v_2 into several A_{ch} intervals allowing for a reduction of the statistical fluctuations.

Understanding the background components and how they contribute to the experimental measurements is crucial to isolate the CMW signal. Among several background sources [58–65], the most dominant one is expected to be the LCC, convoluted with the collective motion of the QGP medium. The LCC mechanism depicts a scenario where pairs of particles with opposite charges are usually generated from resonance decays. Such particle production mechanism is studied with balance function measurements in heavy-ion collisions [66, 67]. In the CMW measurement, when one of the particles from the charge-conserving pair escapes from the limited detector acceptance, a non-zero A_{ch} is consequently generated [58]. It is demonstrated in Ref. [68] that the selection of specific A_{ch} values automatically biases the $\eta-p_{\text{T}}$ phase space. This can trivially give rise to a $A_{\text{ch}}-\Delta v_2$ correlation because of the v_2 dependence on η and p_{T} leading to non-zero slopes, even in absence of CMW phenomena. Theoretical studies on $A_{\text{ch}}-\Delta v_2$ correlations, without the CMW process, have been extensively investigated in Refs. [69–73].

The consensus is that the LCC interpretation can effectively explain both the observed $A_{\text{ch}}-\Delta v_3$ and $A_{\text{ch}}-\Delta v_2$ relations. A pure LCC mechanism is expected to lead to an identical [53, 58] positive linear correlation between $A_{\text{ch}}-\Delta v_2^{\text{Norm}}$ and $A_{\text{ch}}-\Delta v_3^{\text{Norm}}$. Consequently, this implies that any difference between the normalized slopes r_2^{Norm} and r_3^{Norm} may indicate the existence of the CMW signal.

Although there are several measurements of CMW at LHC energies, there is lack of measurements with identified hadrons. Given that the predominant background influence on CMW arises from the interplay of LCC and elliptic flow (v_2), it would be useful to measure the CMW for identified particles, as it would provide us a better handle to control the background related to v_2 [42]. The first theoretical study [42] predicted that only light quarks, i.e., u and d, are influenced by the chiral anomaly. However, recent theoretical calculations [74] suggest that the mass difference between the strange quark (s) and the u, d quarks can be neglected, indicating the possibility of exploring CMW effects with charged kaons. Nevertheless, the significant differences in the absorption cross section for (anti-)protons and kaons in the hadronic matter might obscure the signal. Additionally, a hydrodynamic study [62] suggests that the isospin chemical potential (μ_I) and the strangeness chemical potential (μ_S) can play essential roles. This study predicts a negative slope for kaons at RHIC energies [62]. Therefore, it is difficult to disentangle the CMW signal and various background contributions, if the measurements are performed only with inclusive charged hadrons.

This paper presents the first measurement of normalized slopes r_2^{Norm} and r_3^{Norm} for charged hadrons and identified π^\pm , K^\pm , and $p+\bar{p}$ in Pb–Pb collisions at $\sqrt{s_{\text{NN}}} = 5.02$ TeV. These measurements will provide experimental input to the ongoing theoretical developments for the flavor dependence of the chiral anomalies. Measurements from data are further compared with a recently developed blast wave model calculation, incorporating the LCC background (BW+LCC) [75]. The measurement of integral covariance is also utilized to estimate an upper limit on the CMW contribution, for the first time, in Pb–Pb collisions at $\sqrt{s_{\text{NN}}} = 5.02$ TeV.

This article is organized as follows: Section 2 briefly describes the experimental setup, while Section 3 discusses the data sample, the selection criteria, and the analysis details. Section 4 describes the evaluation of the systematic uncertainties. The results are discussed and compared with model calculations in Section 5. A summary is outlined in Section 6.

2 Experimental apparatus and data sample

The ALICE detector and its performance are described in detail in Refs. [76, 77]. The apparatus consists of a central barrel at midrapidity ($|\eta| < 0.9$), embedded in a cylindrical solenoid which provides a magnetic field of 0.5 T parallel to the beam direction, and a set of forward detectors.

Charged particles produced in the collisions at midrapidity are tracked by the Inner Tracking System (ITS) [76] and the Time Projection Chamber (TPC) [78]. The ITS, composed of the Silicon Pixel Detector (SPD), Silicon Drift Detector (SDD), and Silicon Strip Detector (SSD), consists of six cylindrical silicon layers surrounding the beam vacuum pipe. The TPC, surrounding the ITS, provides up to 159 points for track reconstruction along with specific energy loss (dE/dx) measurements, which are utilized for charged-particle identification (PID). The PID is complemented by a Time-Of-Flight (TOF) detector [79], which measures the flight time of charged particles. The TOF detector provides pion–kaon separation at 3σ level up to $p_T \simeq 2.5$ GeV/ c and pion–proton separation up to $p_T \simeq 4$ GeV/ c .

On either sides of the interaction point, the V0 scintillator arrays [80], are used for triggering and event classification. The V0 detector consists of two arrays of 32 scintillator tiles covering the pseudorapidity ranges $2.8 < \eta < 5.1$ (V0A) and $-3.7 < \eta < -1.7$ (V0C). Both V0 detectors are segmented in four rings in the radial direction with each ring divided into eight sectors in the azimuthal direction. The V0C is also used for ESE and event selection. Two tungsten-quartz neutron Zero Degree Calorimeters

(ZDCs) [76], positioned 112.5 meters from the interaction point on each side, are used to reduce the contamination from beam-induced background. Using the time information from V0 and ZDC, offline event selection is performed to reject background from beam–gas collisions, from parasitic beam–beam interactions, and pileup events [77, 81].

The analysis is performed using the data sample collected with the ALICE apparatus in the 2018 LHC Pb–Pb run at $\sqrt{s_{NN}} = 5.02$ TeV. The centrality intervals were defined in terms of percentiles of the hadronic Pb–Pb cross section, determined from selections on the sum of the V0 signal amplitudes [82]. Central and semicentral Pb–Pb collisions were selected online by applying thresholds on the V0 signal amplitudes resulting in two separate trigger classes (central and semicentral triggers).

Only events with a reconstructed primary vertex located between ± 10 cm with respect to the nominal interaction point along the beam direction (z axis of the ALICE reference frame) are considered. The analysis is performed in different centrality intervals spanning from 0–5% which corresponds to the most central collisions to 50–60% corresponding to peripheral collisions. The total number of analyzed events after the event selection is approximately 240 million.

3 Analysis procedure

Charged particles reconstructed using the TPC and the ITS information within $|\eta| < 0.8$ and $0.2 < p_T < 10$ GeV/ c are considered to determine A_{ch} . For the measurement of flow coefficients, charged particles are restricted to $0.2 < p_T < 2.0$ GeV/ c . Tracks are selected requiring $|\eta| < 0.8$, at least 70 (out of a maximum of 159) TPC space points, and χ^2 per TPC cluster < 2.5 for the momentum fit in the TPC. In order to reduce the contamination from secondary particles (i.e., particles originating from weak decays, conversions, and secondary hadronic interactions in the detector material) only tracks with a maximum distance of closest approach (DCA) to the reconstructed primary vertex in the transverse ($|DCA_{xy}| < 2.4$ cm) and the longitudinal directions ($|DCA_z| < 3.2$ cm) are accepted. Furthermore, tracks are required to have at least one hit in the two SPD layers. Charged pions, kaons, and (anti)protons are identified from the difference between the measured and expected values of dE/dx in TPC and time of flight to the TOF detector, expressed in units of resolution ($|n\sigma|_{TPC}$, $|n\sigma|_{TOF}$), and applying a selection on the number of accepted $n\sigma$ (see Table 1). Additionally, tracks without TOF information with p_T larger than 0.5 GeV/ c for pions, 0.45 GeV/ c for kaons, and 0.6 GeV/ c for protons are rejected. All particle species are required to lie within the rapidity range $|y| < 0.5$. By applying these selection criteria, the efficiency of identifying charged hadrons is approximately 70% around $p_T = 0.5$ GeV/ c and increases to about 80% for p_T values above 1 GeV/ c . Moreover, these selection criteria guarantee a purity exceeding 90% for all particle species across the entire range of p_T values considered in the analysis.

An example of the measured raw A_{ch} distribution is shown in the left panel of Fig. 1 for the 40–50% centrality interval. The raw A_{ch} distribution is divided into ten A_{ch} intervals, each roughly containing equal number of events. The edges of the ten A_{ch} classes are displayed by the dashed lines in the left panel of Fig. 1. The raw A_{ch} is corrected to account for the limited detector acceptance and the reconstruction and identification efficiency of charged hadrons. Using simulations based on the HIJING event generator [83] combined with the GEANT3 model [84] for particle transport in the detector material, a correlation is built between the raw and the true values of A_{ch} [55]. A linear fit to this correlation is performed and the fit function is used to map the raw A_{ch} to the true A_{ch} as shown in the right panel of Fig. 1.

Within each A_{ch} interval, the flow coefficients v_2 and v_3 are measured separately for positively and negatively (identified and inclusive) charged hadrons. The measurements are performed using the two-particle cumulant method [85] with a pseudorapidity gap of $|\Delta\eta| > 0.4$ to suppress non-flow, i.e. correlations not related to the reaction plane [86]. The normalized slope parameters, r_2^{Norm} and r_3^{Norm} , are then calculated for various centrality intervals with Eq. 5 using the values of A_{ch} corrected for detector effects as

described above.

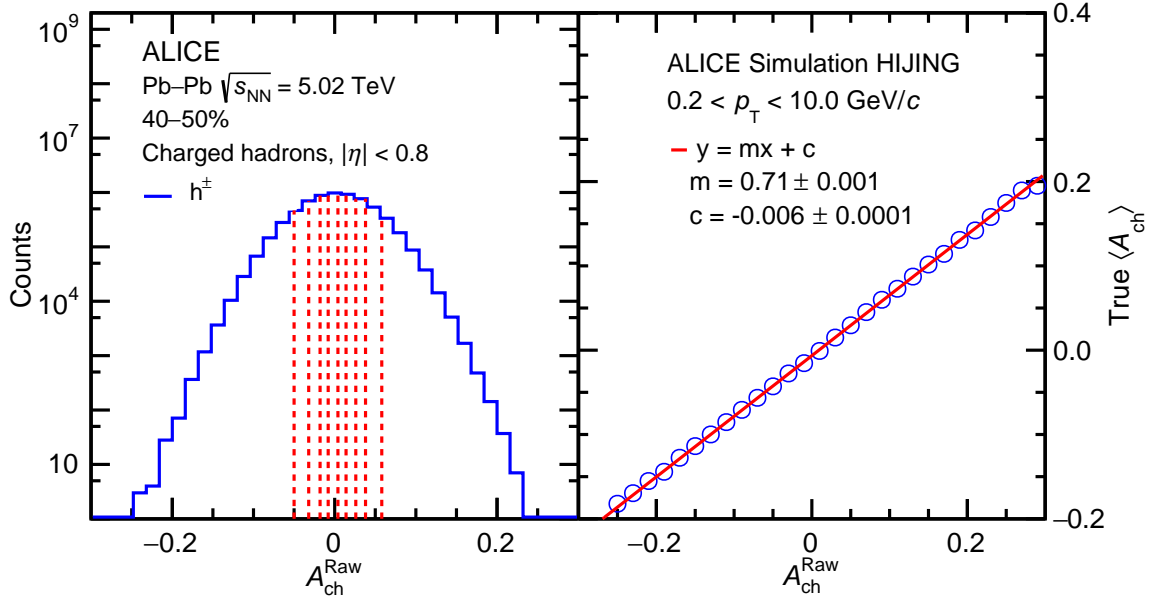


Figure 1: (Left panel): Raw A_{ch} distribution in Pb–Pb collisions at $\sqrt{s_{\text{NN}}} = 5.02$ TeV for the 40–50% centrality interval. Red dotted lines depict the edges of the ten A_{ch} classes. (Right panel): Correlation between true and raw A_{ch} obtained from HIJING simulations combined with a GEANT3 detector model for Pb–Pb collisions at $\sqrt{s_{\text{NN}}} = 5.02$ TeV in the 40–50% centrality interval.

The ESE technique is further employed to estimate possible CMW signal contribution to the ΔIC as proposed in Ref. [56]. In particular, the residual magnitude of this observable when v_2 goes to zero can be used to disentangle the potential CMW signal from the background contributions [33]. The second-order reduced flow vector q_2 is used for event shape selection as in Ref. [33]. It is defined as

$$q_2 = Q_2 / \sqrt{M}, \quad (7)$$

where Q_2 is the magnitude of the flow vector and M is the multiplicity. The Q_2 is calculated from the azimuthal distribution of the energy deposited in the V0C detector. In order to account for a non-uniform detector response, the V0 detector is calibrated using two procedures: gain equalization and recentering. The former flattens the mean multiplicity distribution of the eight azimuthal sectors in each ring, while the latter corrects for systematic shifts of the mean values of the Q_2 vector components [48]. For each centrality interval, ten q_2 ranges are explored, ranging from the most elliptic to the most isotropic event classes.

To separate the LCC background contributions from the potential CMW signal, the dependence of the ΔIC on v_2 (defined in Section 1) is fitted with a linear function. The CMW fraction to the ΔIC is then obtained by the ratio between the observable at zero v_2 and at finite v_2

$$f_{\text{CMW}} \equiv \frac{b}{a \langle v_2 \rangle + b}, \quad (8)$$

where a and b are the slope and the intercept of the linear function, respectively, and $\langle v_2 \rangle$ is the average value over the measured v_2 range.

4 Systematic uncertainties

To estimate the systematic uncertainties on the normalized slopes and f_{CMW} , the event and track selection criteria are varied from their nominal values. Table 1 provides a list of variables used in the selections along with their default and varied values. These include modifying the range of z coordinate of the primary vertex (V_z) from $|V_z| \leq 10$ cm to $|V_z| \leq 8$ cm to examine the detector acceptance dependence. The impact of the track-quality selections is evaluated by changing the minimum number of TPC space points from 70 to 80 and varying the χ^2_{TPC} per TPC space point from 2.5 to 2.0. To test the influence of the contamination from secondary particles on the measurement, tighter selection criteria than the nominal ones are applied to both DCA_{xy} and DCA_z . To estimate the effects of non-flow contributions, the pseudorapidity gap ($\Delta\eta$) is varied from $|\Delta\eta| \geq 0.4$ to $|\Delta\eta| \geq 0.6$ for charged hadrons and pions, and to $|\Delta\eta| \geq 0.5$ for kaons and protons. Particle identification criteria, namely $|n\sigma|_{\text{TPC}}$ and $|n\sigma|_{\text{TOF}}$, are also subject to variations to account for potential systematic effects in the particle identification process and their impact on the final analysis results. The reconstruction efficiency for charged hadrons is calculated using only pions, kaons, and protons and the differences observed in the results are incorporated as systematic uncertainties. For each systematic variation, the corrections for the non-uniform acceptance and for the reconstruction efficiency of inclusive and identified charged hadrons are estimated using collision data and MC simulations. To identify the statistically significant systematic sources, the ratio $B = Y/\sigma_B$ is calculated, where Y represents the difference between the results with the default and the modified selections, and σ_B is the error of the difference estimated as $\sqrt{|\sigma_{\text{default}}^2 \pm \sigma_{\text{varied}}^2|}$, where “+” is used for the uncorrelated and “-” for the correlated sources. The statistical uncertainties σ_{default} and σ_{varied} are estimated separately for the results using the default and varied event/particle selection criteria, following a subsampling method, with 20 equally sized independent samples. Each variation that exhibits a significant difference from the nominal result by more than $1\sigma_B$, according to the recommendations from Ref. [87], is considered a source of systematic uncertainty. The total systematic uncertainties are then obtained by summing the different contributions in quadrature.

Table 1: Nominal event and track selection criteria and the corresponding variations used for the estimation of the systematic uncertainties.

(No.) Source	Default Value	Variations
(1) Primary $ V_z $	< 10 cm	< 8 cm
(2) TPC space points	> 70	> 80
(3) $\chi^2_{\text{TPC}}/\text{cluster}$	< 2.5	< 2.0
(4) DCA_{xy} (DCA_z)	< 2.4 (3.2) cm	< 7(0.0026 + (0.005/ $p_T^{1.01}$)), (2.0) cm
(5) $ \Delta\eta $	> 0.4	> 0.6 (0.5 for K and p)
(6) PID (π)	-	-
0.2 < p_T < 0.5 (GeV/c)	$ n\sigma _{\text{TPC}} < 3$	$ n\sigma _{\text{TPC}} < 2.5$
0.5 < p_T < 2.0 (GeV/c)	$\sqrt{ n\sigma _{\text{TPC}}^2 + n\sigma _{\text{TOF}}^2} < 3$	$\sqrt{ n\sigma _{\text{TPC}}^2 + n\sigma _{\text{TOF}}^2} < 3$
PID (K)	-	-
0.2 < p_T < 0.45 (GeV/c)	$ n\sigma _{\text{TPC}} < 3$	$ n\sigma _{\text{TPC}} < 2.5$
0.45 < p_T < 2.0 (GeV/c)	$\sqrt{ n\sigma _{\text{TPC}}^2 + n\sigma _{\text{TOF}}^2} < 2.5$	$\sqrt{ n\sigma _{\text{TPC}}^2 + n\sigma _{\text{TOF}}^2} < 2$
PID (p)	-	-
0.5 < p_T < 0.6 (GeV/c)	$ n\sigma _{\text{TPC}} < 3$	$ n\sigma _{\text{TPC}} < 3.5$
0.6 < p_T < 2.0 (GeV/c)	$\sqrt{ n\sigma _{\text{TPC}}^2 + n\sigma _{\text{TOF}}^2} < 3.0$	$\sqrt{ n\sigma _{\text{TPC}}^2 + n\sigma _{\text{TOF}}^2} < 3.5$
(7) Efficiency calculation	All unidentified charged hadrons	Identified charged hadrons (π +K+p)

Table 2 summarizes the maximum magnitude of the systematic uncertainties on the normalized slopes

over all the centrality intervals from each individual source which passes the criteria described above. The systematic sources for the f_{CMW} observable are only a few, namely Primary V_z , $\chi_{\text{TPC}}^2/\text{cluster}$, and DCA selections. The associated uncertainties are 0.024, 0.047, and 0.068, respectively.

Table 2: Maximum systematic uncertainty (absolute value) on normalized slope per particle species over all centrality intervals from individual sources (see Table 1 for an explanation of each source).

Sources	inclusive (h^\pm)		π^\pm		K^\pm		$p+\bar{p}$	
	r_2^{Norm}	r_3^{Norm}	r_2^{Norm}	r_3^{Norm}	r_2^{Norm}	r_3^{Norm}	r_2^{Norm}	r_3^{Norm}
(1) Primary V_z	0.014	0.03	0.012	0.03	0.019	0.12	0.02	0.021
(2) TPC space points	0.003	0.033	0.01	0.033	0.033	0.23	0.036	0.14
(3) $\chi_{\text{TPC}}^2/\text{cluster}$	0.009	0.047	0.0002	0.047	0.02	0.31	0.035	0.18
(4) DCA_{xy} (DCA_z)	0.005	0.044	0.023	0.044	0.02	0.18	0.026	0.19
(5) $ \Delta\eta $	0.013	0.09	0.018	0.09	0.017	0.31	0.052	0.11
(6) PID	-	-	0.05	0.05	0.013	0.11	0.004	0.13
(7) Efficiency	0.032	0.049	-	-	-	-	-	-

5 Results

5.1 A_{ch} dependence of v_n and centrality dependence of the slope r_n^{Norm}

The top left and top right panels of Fig. 2 show, respectively, the v_2 and v_3 of positively and negatively charged hadrons as a function of A_{ch} for Pb–Pb collisions at $\sqrt{s_{\text{NN}}} = 5.02$ TeV in the 40–50% centrality interval. A significant decreasing (increasing) trend of v_2 for positively (negatively) charged hadrons as a function of A_{ch} is observed. Such trends are also present for the v_3 coefficient though the fluctuations are larger. In Fig. 2 the correlated uncertainties between the hadrons and among A_{ch} intervals are represented with shaded bands. The normalized difference between the v_2 and v_3 of positive and negative charged particles, as defined in Eq. 5, is shown as a function of A_{ch} in the bottom left and right panels of Fig. 2, respectively. They are fitted with linear functions to obtain the slopes, r_2^{Norm} and r_3^{Norm} . In addition to a positive slope for $\Delta v_2/\langle v_2 \rangle$, a non-zero slope is also found for $\Delta v_3/\langle v_3 \rangle$ (i.e., $r_3^{\text{Norm}} > 0$), which mainly contains the background correlations. This non-zero r_3^{Norm} indicates that similar background is also present in r_2^{Norm} which need to be subtracted to make a quantitative measurement of CMW. Note that the difference in non-flow contributions to same-sign and opposite-sign pairs can induce a trivial correlation between v_n and A_{ch} [55, 88]. However, it is estimated that this trivial correlation is negligible at this collision energy. Figure 3 shows r_2^{Norm} (red markers) and r_3^{Norm} (green markers) as a function of centrality for inclusive charged hadrons in Pb–Pb collisions at $\sqrt{s_{\text{NN}}} = 5.02$ TeV. Despite the large uncertainties, r_3^{Norm} seems to be of similar magnitude to r_2^{Norm} , for most of the centrality range. The CMW is expected to develop in the direction of the magnetic field \mathbf{B} , i.e., approximately perpendicular to the second order event plane rather than the third order. The third order plane has very little correlation with the second order event plane [89–91]. Hence, the non-zero r_3^{Norm} value cannot originate from the CMW-induced electric quadrupole moment, but it should rather be attributed to the LCC mechanism. Thus, the similarity between the magnitudes of r_2^{Norm} and r_3^{Norm} could indicate that both of them are mainly dominated by the LCC background. The results are also in good agreement with the CMS measurements for the same collision system and energy [53]. While the precision of the CMS measurements is notable, the findings presented in this study expand the scope of measurements to encompass the most central collision scenarios. The r_2^{Norm} is further compared with a blast wave model calculation (green band) which takes into account the LCC effect [75]. This model uses blast wave parameters obtained from the simultaneous fit of p_{T} -differential yields and v_2 of identified particles from Pb–Pb collisions at $\sqrt{s_{\text{NN}}} = 5.02$ TeV [81]. Then, the model distributes source points within an ellipsoid (defined by the blast wave parameter) from where it produces oppositely charged particles (i.e. balancing charges). The number of sources is tuned in such a way that the A_{ch} distribution from the output of the model matches with the experimental data. Then, the normalized slope values are calculated from the model, following the

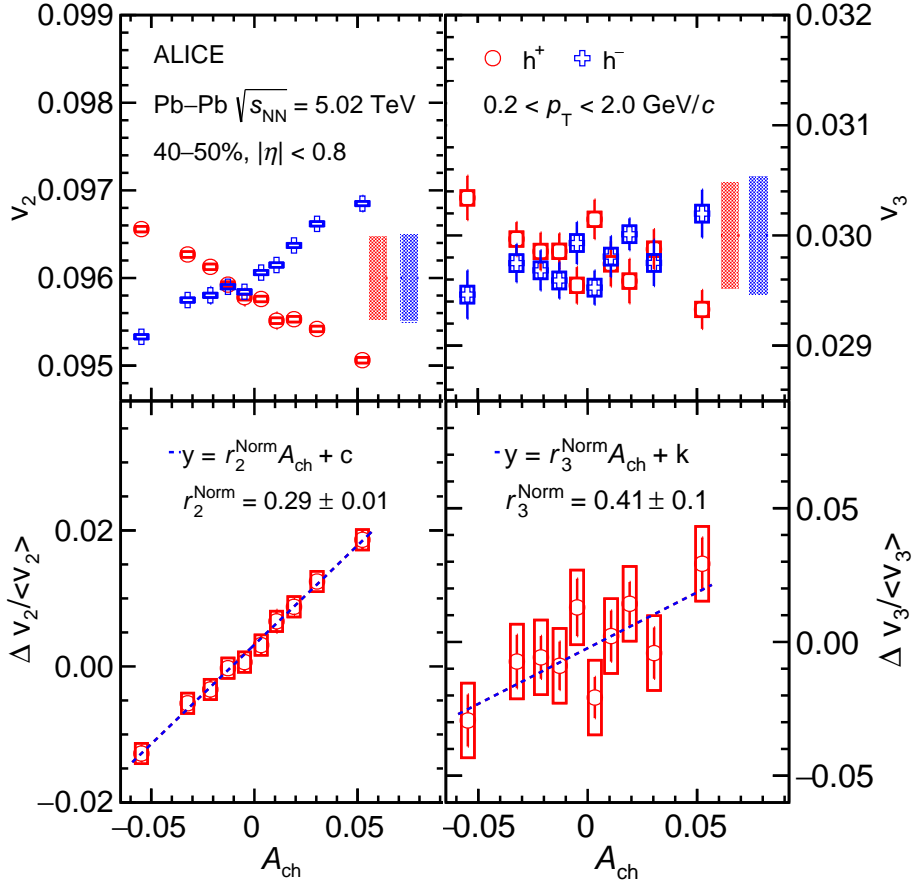


Figure 2: The top left panel shows the v_2 of positively (red markers) and negatively (blue markers) charged hadrons as a function of the corrected A_{ch} , while the top right panel shows the same for v_3 . Statistical uncertainties are shown by bars and uncorrelated (correlated) systematic uncertainties by open boxes (shaded bands). The bottom left panel shows $\Delta v_2 / \langle v_2 \rangle$ as a function of the corrected A_{ch} and bottom right panel shows the same for $\Delta v_3 / \langle v_3 \rangle$, all for the 40–50% centrality interval in Pb–Pb collisions at $\sqrt{s_{NN}} = 5.02$ TeV. The dotted blue line shows the linear fit to the data points to obtain the values of normalized slopes (r_2^{Norm} and r_3^{Norm}).

same procedure as in data. The agreement between the model and the experimental results of r_2^{Norm} points to a large background contribution in the measurement. The r_2^{Norm} and r_3^{Norm} results for identified hadrons are shown in Fig. 4 as a function of centrality. For r_2^{Norm} , the slope for kaons behaves similarly as the slope for pions, while the slope for protons slightly differs with a weak A_{ch} – Δv_2 dependence on centrality. In the 20% most central collisions, a hint of mass ordering is observed, i.e., the slopes of pions are slightly larger than those of kaons, and the slopes of kaons are slightly larger than those of protons. However, the uncertainties are too large for a definitive conclusion to be made. The LCC process, the dominant background for this measurement, can reproduce the measurement of r_2^{Norm} in data. Therefore, it is expected that the mass ordering of v_2 of identified particles might be the reason behind the apparent particle type dependence of r_2^{Norm} seen in Fig. 4. This finding contradicts the predictions of the hydrodynamic study, which anticipated negative slopes for kaons and protons [62]. A similar behavior is found in the STAR CMW measurement at a lower collision energy, in which the isospin and strangeness chemical potentials and the different absorption cross section are expected to play a role [55, 62, 92]. However, at LHC energies, the values of the chemical potentials are close to zero, suggesting that their influence should be negligible. For r_3^{Norm} , the slopes of all the measured hadron species are compatible with each other within the uncertainties. Since no predictions for the CMW for different particle species are available at LHC energies, the results shown here provide, for the first time, an experimental input

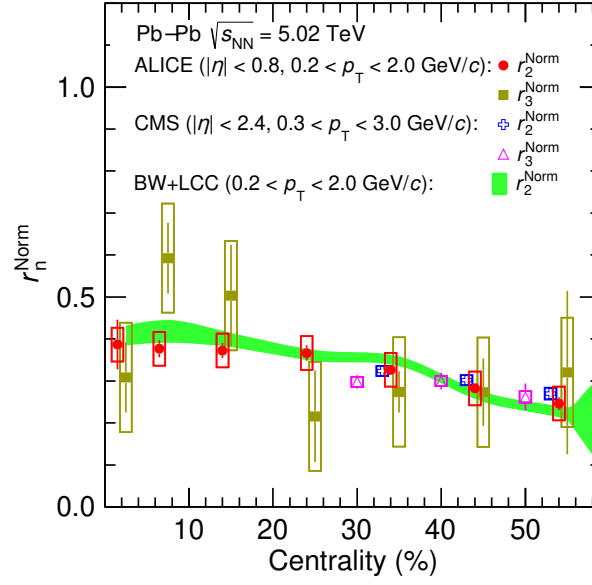


Figure 3: Centrality dependence of normalized slopes r_2^{Norm} and r_3^{Norm} for inclusive charged hadrons in Pb–Pb collisions at $\sqrt{s_{NN}} = 5.02$ TeV compared with CMS results [53] and a BW+LCC model calculation [75]. Statistical (systematic) uncertainties are depicted by bars (boxes). ALICE r_2^{Norm} and r_3^{Norm} and CMS r_2^{Norm} data points are slightly shifted horizontally for visibility.

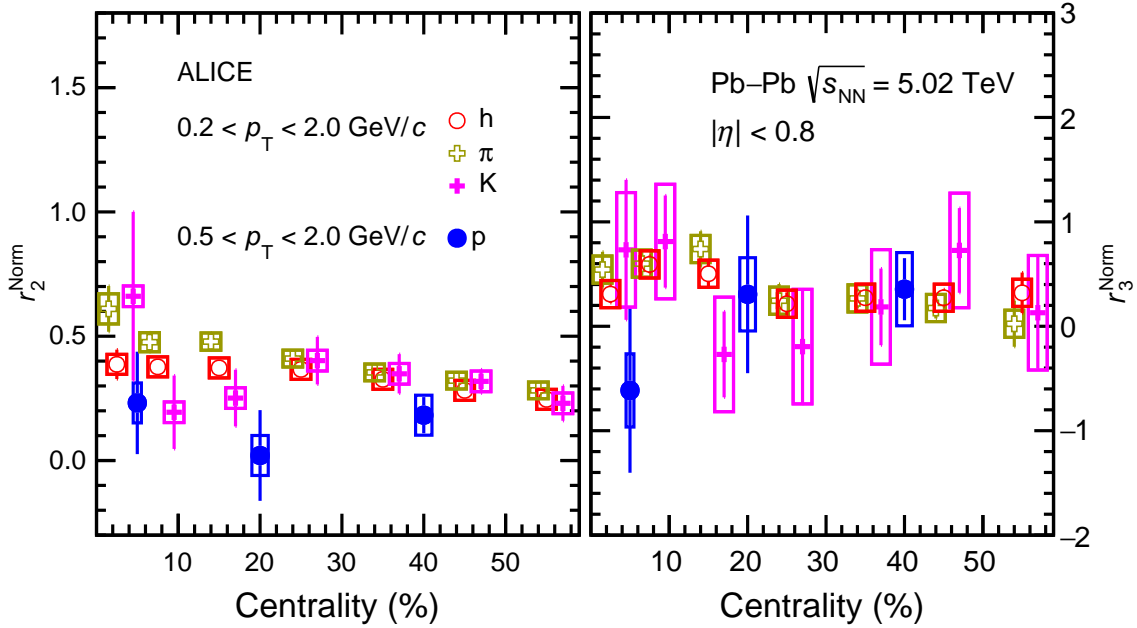


Figure 4: Centrality dependence of normalized slopes r_2^{Norm} (left panel) and r_3^{Norm} (right panel) for inclusive and identified charged hadrons in Pb–Pb collisions at $\sqrt{s_{NN}} = 5.02$ TeV. Statistical (systematic) uncertainties are depicted by bars (boxes). The data points for charged pions and kaons are slightly shifted horizontally for visibility.

for theoretical calculations.

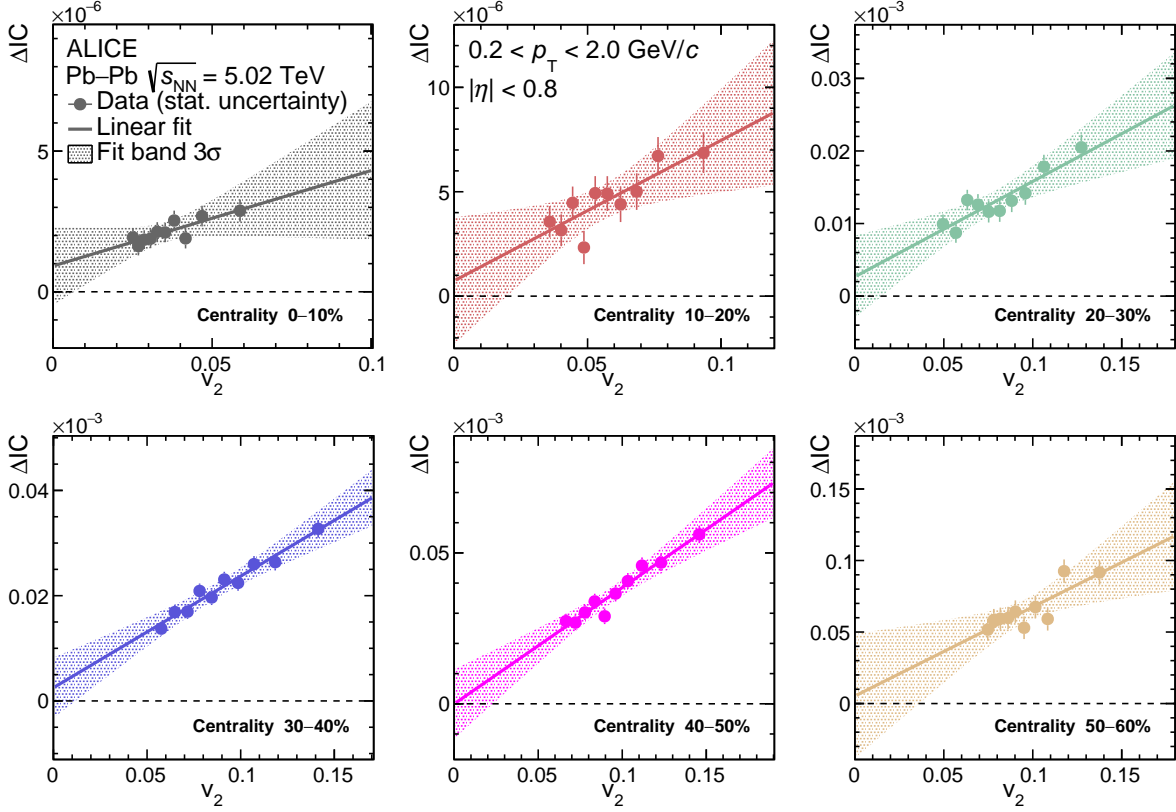


Figure 5: Dependence of ΔIC on v_2 of shape-selected events from the 0–10% (top left panel) to the 50–60% (bottom right panel) centrality intervals of Pb–Pb collisions at $\sqrt{s_{NN}} = 5.02$ TeV. The solid lines are straight line fit to the data points. Only statistical uncertainties are shown. The bands represent the three standard deviation uncertainties from the linear fit.

5.2 Constraining the fraction of the CMW with the ESE

Figure 5 shows the difference of the integrated covariance ΔIC as a function of v_2 for q_2 -selected events in six centrality intervals. Solid lines, representing linear fits, and colored bands, denoting three standard deviation uncertainties of the linear fits are also shown. The ΔIC values exhibit a decrease as v_2 approaches zero, as discussed in Ref. [56]. The small magnitude of the intercepts in all centrality intervals indicates that the measurement is dominated by the LCC background.

After obtaining the slope and intercept from the fit of ΔIC as a function of v_2 , the fraction of the CMW signal, denoted as f_{CMW} , can be determined using Eq. 8. The centrality dependence of f_{CMW} is presented in Fig. 6 where the error bars display the statistical uncertainties extracted from the fits of Fig. 5. Meaningful measurements are not possible in the most central and peripheral collisions, due to the small v_2 values and the large statistical fluctuations. Therefore, the f_{CMW} results are reported only in the 10–60% centrality range. The systematic uncertainties are estimated for the different possible sources, as discussed in Sec. 4. The systematic sources, which are found to be significant among centrality intervals, are combined in quadrature and shown as a dark shaded band in Fig. 6, at centrality around 60%. It is found that the f_{CMW} is consistent with zero within the reported statistical and systematic uncertainties.

The f_{CMW} data points in Fig. 6 are fitted with a constant, yielding a value of $f_{CMW} = 0.081 \pm 0.055$ (the dashed blue line), which should be combined with the systematic uncertainty of 0.087 (the gray box on the edge) to establish an upper limit on f_{CMW} of 26% (38%) at 95% (99.7%) confidence level shown by the dotted magenta line. This result provides the first quantitative assessment of the upper limit of the fraction of the Chiral Magnetic Wave (CMW) at the top LHC energy.

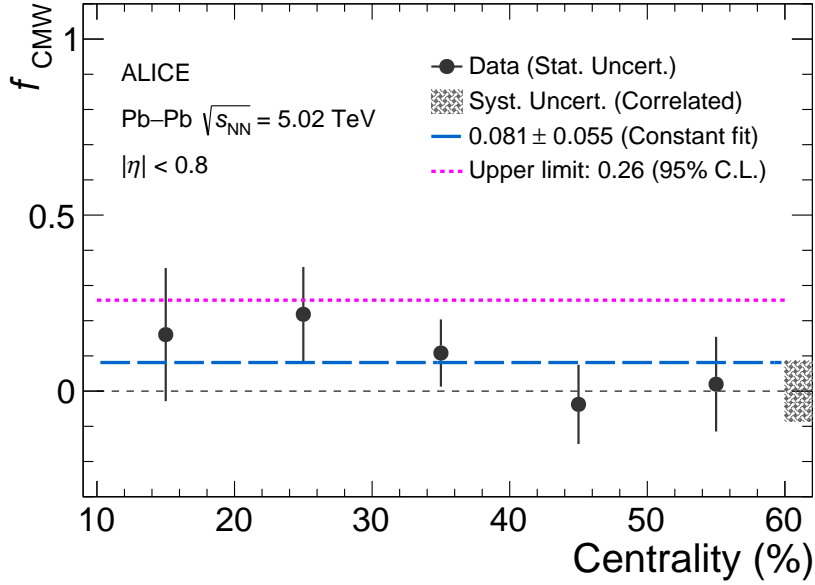


Figure 6: Centrality dependence of the extracted CMW fraction. The 95% confidence level of the upper limit is also shown by the dotted magenta line. Statistical uncertainties are depicted by bars, while the correlated systematic uncertainty is represented by a shaded band on the right edge. The blue line is the constant fit line of the data points.

6 Summary

The difference between the v_2 and v_3 coefficients of positively and negatively charged particles are measured as a function of the charge asymmetry A_{ch} for inclusive and identified hadrons in Pb–Pb collisions at $\sqrt{s_{\text{NN}}} = 5.02$ TeV. The slopes r_2^{Norm} and r_3^{Norm} are found to be consistent with each other within the reported uncertainties, suggesting that the dominant contribution to r_2^{Norm} is not due to CMW. A blast wave parameterization that incorporates local charge conservation, tuned to reproduce the A_{ch} distribution, is able to fully describe the magnitude of r_2^{Norm} which is expected to be sensitive to CMW. Additionally, a hint for mass ordering of the r_2^{Norm} slopes of pions, kaons, and protons is discernible in the most central collisions, though it is accompanied by large uncertainties. Furthermore, using the Event Shape Engineering (ESE) technique, both the fraction and the upper limit of the CMW signal are extracted. Averaging over the 10–60% centrality interval, the CMW fraction is consistent with zero within uncertainties and an upper limit of 26% (38%) is estimated at 95% (99.7%) confidence level.

Acknowledgements

The ALICE Collaboration would like to thank all its engineers and technicians for their invaluable contributions to the construction of the experiment and the CERN accelerator teams for the outstanding performance of the LHC complex. The ALICE Collaboration gratefully acknowledges the resources and support provided by all Grid centres and the Worldwide LHC Computing Grid (WLCG) collaboration. The ALICE Collaboration acknowledges the following funding agencies for their support in building and running the ALICE detector: A. I. Alikhanyan National Science Laboratory (Yerevan Physics Institute) Foundation (ANSL), State Committee of Science and World Federation of Scientists (WFS), Armenia; Austrian Academy of Sciences, Austrian Science Fund (FWF): [M 2467-N36] and Nationalstiftung für Forschung, Technologie und Entwicklung, Austria; Ministry of Communications and High Technologies, National Nuclear Research Center, Azerbaijan; Conselho Nacional de Desenvolvimento Científico e Tecnológico (CNPq), Financiadora de Estudos e Projetos (Finep), Fundação de Amparo à Pesquisa do Estado de São Paulo (FAPESP) and Universidade Federal do Rio Grande do Sul (UFRGS), Brazil; Bulgarian Ministry of Education and Science, within the National Roadmap for Research Infras-

tructures 2020–2027 (object CERN), Bulgaria; Ministry of Education of China (MOEC), Ministry of Science & Technology of China (MSTC) and National Natural Science Foundation of China (NSFC), China; Ministry of Science and Education and Croatian Science Foundation, Croatia; Centro de Aplicaciones Tecnológicas y Desarrollo Nuclear (CEADEN), Cubaenergía, Cuba; Ministry of Education, Youth and Sports of the Czech Republic, Czech Republic; The Danish Council for Independent Research | Natural Sciences, the VILLUM FONDEN and Danish National Research Foundation (DNRF), Denmark; Helsinki Institute of Physics (HIP), Finland; Commissariat à l’Energie Atomique (CEA) and Institut National de Physique Nucléaire et de Physique des Particules (IN2P3) and Centre National de la Recherche Scientifique (CNRS), France; Bundesministerium für Bildung und Forschung (BMBF) and GSI Helmholtzzentrum für Schwerionenforschung GmbH, Germany; General Secretariat for Research and Technology, Ministry of Education, Research and Religions, Greece; National Research, Development and Innovation Office, Hungary; Department of Atomic Energy Government of India (DAE), Department of Science and Technology, Government of India (DST), University Grants Commission, Government of India (UGC) and Council of Scientific and Industrial Research (CSIR), India; National Research and Innovation Agency - BRIN, Indonesia; Istituto Nazionale di Fisica Nucleare (INFN), Italy; Japanese Ministry of Education, Culture, Sports, Science and Technology (MEXT) and Japan Society for the Promotion of Science (JSPS) KAKENHI, Japan; Consejo Nacional de Ciencia (CONACYT) y Tecnología, through Fondo de Cooperación Internacional en Ciencia y Tecnología (FONCICYT) and Dirección General de Asuntos del Personal Académico (DGAPA), Mexico; Nederlandse Organisatie voor Wetenschappelijk Onderzoek (NWO), Netherlands; The Research Council of Norway, Norway; Commission on Science and Technology for Sustainable Development in the South (COMSATS), Pakistan; Pontificia Universidad Católica del Perú, Peru; Ministry of Education and Science, National Science Centre and WUT ID-UB, Poland; Korea Institute of Science and Technology Information and National Research Foundation of Korea (NRF), Republic of Korea; Ministry of Education and Scientific Research, Institute of Atomic Physics, Ministry of Research and Innovation and Institute of Atomic Physics and University Politehnica of Bucharest, Romania; Ministry of Education, Science, Research and Sport of the Slovak Republic, Slovakia; National Research Foundation of South Africa, South Africa; Swedish Research Council (VR) and Knut & Alice Wallenberg Foundation (KAW), Sweden; European Organization for Nuclear Research, Switzerland; Suranaree University of Technology (SUT), National Science and Technology Development Agency (NSTDA), Thailand Science Research and Innovation (TSRI) and National Science, Research and Innovation Fund (NSRF), Thailand; Turkish Energy, Nuclear and Mineral Research Agency (TENMAK), Turkey; National Academy of Sciences of Ukraine, Ukraine; Science and Technology Facilities Council (STFC), United Kingdom; National Science Foundation of the United States of America (NSF) and United States Department of Energy, Office of Nuclear Physics (DOE NP), United States of America. In addition, individual groups or members have received support from: European Research Council, Strong 2020 - Horizon 2020 (grant nos. 950692, 824093), European Union; Academy of Finland (Center of Excellence in Quark Matter) (grant nos. 346327, 346328), Finland.

References

- [1] W. Busza, K. Rajagopal, and W. van der Schee, “Heavy Ion Collisions: The Big Picture, and the Big Questions”, *Ann. Rev. Nucl. Part. Sci.* **68** (2018) 339–376, arXiv:1802.04801 [hep-ph].
- [2] J. Schukraft, “Ultra-relativistic heavy-ion collisions: Searching for the quark-gluon plasma”, *Nucl. Phys. A* **553** (1993) 31–44.
- [3] U. W. Heinz, “The Strongly coupled quark-gluon plasma created at RHIC”, *J. Phys. A* **42** (2009) 214003, arXiv:0810.5529 [nucl-th].
- [4] E. V. Shuryak, “Quantum Chromodynamics and the Theory of Superdense Matter”, *Phys. Rept.* **61** (1980) 71–158.

- [5] J. C. Collins and M. J. Perry, “Superdense Matter: Neutrons Or Asymptotically Free Quarks?”, *Phys. Rev. Lett.* **34** (1975) 1353.
- [6] ALICE Collaboration, “The ALICE experiment – A journey through QCD”, arXiv:2211.04384 [nucl-ex].
- [7] Y. Aoki, G. Endrodi, Z. Fodor, S. D. Katz, and K. K. Szabo, “The Order of the quantum chromodynamics transition predicted by the standard model of particle physics”, *Nature* **443** (2006) 675–678, arXiv:hep-lat/0611014.
- [8] F. R. Brown et al, “On the existence of a phase transition for QCD with three light quarks”, *Phys. Rev. Lett.* **65** (1990) 2491–2494.
- [9] A. Bzdak and V. Skokov, “Event-by-event fluctuations of magnetic and electric fields in heavy ion collisions”, *Phys. Lett.* **B710** (2012) 171–174, arXiv:1111.1949 [hep-ph].
- [10] T. D. Lee, “A Theory of Spontaneous T Violation”, *Phys. Rev. D* **8** (1973) 1226–1239.
- [11] T. D. Lee and G. C. Wick, “Vacuum Stability and Vacuum Excitation in a Spin 0 Field Theory”, *Phys. Rev.* **D9** (1974) 2291–2316.
- [12] D. Kharzeev, R. D. Pisarski, and M. H. G. Tytgat, “Possibility of spontaneous parity violation in hot QCD”, *Phys. Rev. Lett.* **81** (1998) 512–515, arXiv:hep-ph/9804221 [hep-ph].
- [13] P. D. Morley and I. A. Schmidt, “Strong P, CP, T Violations in Heavy Ion Collisions”, *Z. Phys.* **C26** (1985) 627.
- [14] D. Kharzeev and R. D. Pisarski, “Pionic measures of parity and CP violation in high-energy nuclear collisions”, *Phys. Rev.* **D61** (2000) 111901, arXiv:hep-ph/9906401 [hep-ph].
- [15] D. E. Kharzeev, “The Chiral Magnetic Effect and Anomaly-Induced Transport”, *Prog. Part. Nucl. Phys.* **75** (2014) 133–151, arXiv:1312.3348 [hep-ph].
- [16] D. E. Kharzeev, “Topology, magnetic field, and strongly interacting matter”, *Ann. Rev. Nucl. Part. Sci.* **65** (2015) 193–214, arXiv:1501.01336 [hep-ph].
- [17] D. E. Kharzeev and J. Liao, “Chiral magnetic effect reveals the topology of gauge fields in heavy-ion collisions”, *Nat Rev Phys* **3** (Jan., 2021) 55–63.
<http://www.nature.com/articles/s42254-020-00254-6>.
- [18] S. A. Voloshin, “Parity violation in hot QCD: How to detect it”, *Phys. Rev.* **C70** (2004) 057901, arXiv:hep-ph/0406311 [hep-ph].
- [19] D. Kharzeev and A. Zhitnitsky, “Charge separation induced by P-odd bubbles in QCD matter”, *Nucl. Phys.* **A797** (2007) 67–79, arXiv:0706.1026 [hep-ph].
- [20] K. Fukushima, D. E. Kharzeev, and H. J. Warringa, “The Chiral Magnetic Effect”, *Phys. Rev.* **D78** (2008) 074033, arXiv:0808.3382 [hep-ph].
- [21] D. E. Kharzeev, L. D. McLerran, and H. J. Warringa, “The Effects of topological charge change in heavy ion collisions: ’Event by event P and CP violation’”, *Nucl. Phys.* **A803** (2008) 227–253, arXiv:0711.0950 [hep-ph].
- [22] Q. Li et al, “Observation of the chiral magnetic effect in ZrTe5”, *Nature Phys.* **12** (2016) 550–554, arXiv:1412.6543 [cond-mat.str-el].

- [23] Y.-C. Liu and X.-G. Huang, “Anomalous chiral transports and spin polarization in heavy-ion collisions”, *Nucl. Sci. Tech.* **31** (2020) 56, arXiv:2003.12482 [nucl-th].
- [24] J.-H. Gao, G.-L. Ma, S. Pu, and Q. Wang, “Recent developments in chiral and spin polarization effects in heavy-ion collisions”, *Nucl. Sci. Tech.* **31** (2020) 90, arXiv:2005.10432 [hep-ph].
- [25] **STAR** Collaboration, B. I. Abelev *et al.*, “Azimuthal Charged-Particle Correlations and Possible Local Strong Parity Violation”, *Phys. Rev. Lett.* **103** (2009) 251601, arXiv:0909.1739 [nucl-ex].
- [26] **STAR** Collaboration, B. I. Abelev *et al.*, “Observation of charge-dependent azimuthal correlations and possible local strong parity violation in heavy ion collisions”, *Phys. Rev. C* **81** (2010) 054908, arXiv:0909.1717 [nucl-ex].
- [27] **ALICE** Collaboration, B. Abelev *et al.*, “Charge separation relative to the reaction plane in Pb–Pb collisions at $\sqrt{s_{NN}} = 2.76$ TeV”, *Phys. Rev. Lett.* **110** (2013) 012301, arXiv:1207.0900 [nucl-ex].
- [28] S. Schlichting and S. Pratt, “Charge conservation at energies available at the BNL Relativistic Heavy Ion Collider and contributions to local parity violation observables”, *Phys. Rev.* **C83** (2011) 014913, arXiv:1009.4283 [nucl-th].
- [29] S. Pratt, S. Schlichting, and S. Gavin, “Effects of Momentum Conservation and Flow on Angular Correlations at RHIC”, *Phys. Rev.* **C84** (2011) 024909, arXiv:1011.6053 [nucl-th].
- [30] **STAR** Collaboration, L. Adamczyk *et al.*, “Measurement of charge multiplicity asymmetry correlations in high-energy nucleus-nucleus collisions at $\sqrt{s_{NN}} = 200$ GeV”, *Phys. Rev.* **C89** (2014) 044908, arXiv:1303.0901 [nucl-ex].
- [31] **STAR** Collaboration, L. Adamczyk *et al.*, “Fluctuations of charge separation perpendicular to the event plane and local parity violation in $\sqrt{s_{NN}} = 200$ GeV Au+Au collisions at the BNL Relativistic Heavy Ion Collider”, *Phys. Rev.* **C88** (2013) 064911, arXiv:1302.3802 [nucl-ex].
- [32] **STAR** Collaboration, L. Adamczyk *et al.*, “Beam-energy dependence of charge separation along the magnetic field in Au+Au collisions at RHIC”, *Phys. Rev. Lett.* **113** (2014) 052302, arXiv:1404.1433 [nucl-ex].
- [33] **ALICE** Collaboration, S. Acharya *et al.*, “Constraining the magnitude of the Chiral Magnetic Effect with Event Shape Engineering in Pb–Pb collisions at $\sqrt{s_{NN}} = 2.76$ TeV”, *Phys. Lett.* **B777** (2018) 151–162, arXiv:1709.04723 [nucl-ex].
- [34] **CMS** Collaboration, V. Khachatryan *et al.*, “Observation of charge-dependent azimuthal correlations in p -Pb collisions and its implication for the search for the chiral magnetic effect”, *Phys. Rev. Lett.* **118** (2017) 122301, arXiv:1610.00263 [nucl-ex].
- [35] **STAR** Collaboration, J. Adam *et al.*, “Charge-dependent pair correlations relative to a third particle in $p + Au$ and $d + Au$ collisions at RHIC”, *Phys. Lett.* **B798** (2019) 134975, arXiv:1906.03373 [nucl-ex].
- [36] **CMS** Collaboration, A. M. Sirunyan *et al.*, “Constraints on the chiral magnetic effect using charge-dependent azimuthal correlations in pPb and $PbPb$ collisions at the CERN Large Hadron Collider”, *Phys. Rev.* **C97** (2018) 044912, arXiv:1708.01602 [nucl-ex].
- [37] W. Li and G. Wang, “Chiral Magnetic Effects in Nuclear Collisions”, *Annu. Rev. Nucl. Part. Sci.* **70** (Oct., 2020) 293–321.
<https://www.annualreviews.org/doi/10.1146/annurev-nucl-030220-065203>.

- [38] **STAR** Collaboration, J. Adam *et al.*, “Methods for a blind analysis of isobar data collected by the STAR collaboration”, *Nucl. Sci. Tech.* **32** (2021) 48, arXiv:1911.00596 [nucl-ex].
- [39] **STAR** Collaboration, M. S. Abdallah *et al.*, “Search for the chiral magnetic effect with isobar collisions at $\sqrt{s_{NN}} = 200$ GeV by the STAR Collaboration at the BNL Relativistic Heavy Ion Collider”, *Phys. Rev. C* **105** (Jan., 2022) 014901.
<https://link.aps.org/doi/10.1103/PhysRevC.105.014901>.
- [40] D. T. Son and A. R. Zhitnitsky, “Quantum anomalies in dense matter”, *Phys. Rev. D* **70** (2004) 074018, arXiv:hep-ph/0405216.
- [41] M. A. Metlitski and A. R. Zhitnitsky, “Anomalous axion interactions and topological currents in dense matter”, *Phys. Rev. D* **72** (2005) 045011, arXiv:hep-ph/0505072.
- [42] Y. Burnier, D. E. Kharzeev, J. Liao, and H.-U. Yee, “Chiral magnetic wave at finite baryon density and the electric quadrupole moment of quark-gluon plasma in heavy ion collisions”, *Phys. Rev. Lett.* **107** (2011) 052303, arXiv:1103.1307 [hep-ph].
- [43] Y. Burnier, D. E. Kharzeev, J. Liao, and H. U. Yee, “From the chiral magnetic wave to the charge dependence of elliptic flow”, arXiv:1208.2537 [hep-ph].
- [44] D. E. Kharzeev and H.-U. Yee, “Chiral Magnetic Wave”, *Phys. Rev. D* **83** (2011) 085007, arXiv:1012.6026 [hep-th].
- [45] H.-U. Yee and Y. Yin, “Realistic Implementation of Chiral Magnetic Wave in Heavy Ion Collisions”, *Phys. Rev. C* **89** (2014) 044909, arXiv:1311.2574 [nucl-th].
- [46] S. F. Taghavi and U. A. Wiedemann, “Chiral magnetic wave in an expanding QCD fluid”, *Phys. Rev. C* **91** (2015) 024902, arXiv:1310.0193 [hep-ph].
- [47] S. Voloshin and Y. Zhang, “Flow study in relativistic nuclear collisions by Fourier expansion of Azimuthal particle distributions”, *Z. Phys.* **C70** (1996) 665–672, arXiv:hep-ph/9407282 [hep-ph].
- [48] A. M. Poskanzer and S. A. Voloshin, “Methods for analyzing anisotropic flow in relativistic nuclear collisions”, *Phys. Rev. C* **58** (1998) 1671–1678, arXiv:nucl-ex/9805001 [nucl-ex].
- [49] M. Wang, J.-Q. Tao, H. Zheng, W.-C. Zhang, L.-L. Zhu, and A. Bonasera, “Number-of-constituent-quark scaling of elliptic flow: a quantitative study”, *Nucl. Sci. Tech.* **33** (Mar., 2022) 37. <https://link.springer.com/10.1007/s41365-022-01019-9>.
- [50] **STAR** Collaboration, L. Adamczyk *et al.*, “Observation of charge asymmetry dependence of pion elliptic flow and the possible chiral magnetic wave in heavy-ion collisions”, *Phys. Rev. Lett.* **114** (2015) 252302, arXiv:1504.02175 [nucl-ex].
- [51] **ALICE** Collaboration, J. Adam *et al.*, “Charge-dependent flow and the search for the chiral magnetic wave in Pb–Pb collisions at $\sqrt{s_{NN}} = 2.76$ TeV”, *Phys. Rev. C* **93** (2016) 044903, arXiv:1512.05739 [nucl-ex].
- [52] W.-T. Deng and X.-G. Huang, “Event-by-event generation of electromagnetic fields in heavy-ion collisions”, *Phys. Rev. C* **85** (2012) 044907, arXiv:1201.5108 [nucl-th].
- [53] **CMS** Collaboration, A. M. Sirunyan *et al.*, “Probing the chiral magnetic wave in *pPb* and *PbPb* collisions at $\sqrt{s_{NN}} = 5.02$ TeV using charge-dependent azimuthal anisotropies”, *Phys. Rev. C* **100** (2019) 064908, arXiv:1708.08901 [nucl-ex].

- [54] R. Belmont and J. L. Nagle, “Implications of p+Pb measurements on the chiral magnetic effect in heavy ion collisions”, *Phys. Rev. C* **96** (2017) 024901, arXiv:1610.07964 [nucl-th].
- [55] **STAR** Collaboration, M. I. Abdulhamid *et al.*, “Search for the chiral magnetic wave using anisotropic flow of identified particles at energies available at the BNL Relativistic Heavy Ion Collider”, *Phys. Rev. C* **108** (2023) 014908, arXiv:2210.14027 [nucl-ex].
- [56] C.-Z. Wang, W.-Y. Wu, Q.-Y. Shou, G.-L. Ma, Y.-G. Ma, and S. Zhang, “Interpreting the charge-dependent flow and constraining the chiral magnetic wave with event shape engineering”, *Phys. Lett. B* **820** (2021) 136580, arXiv:2104.05551 [nucl-th].
- [57] J. Schukraft, A. Timmins, and S. A. Voloshin, “Ultra-relativistic nuclear collisions: event shape engineering”, *Phys. Lett.* **B719** (2013) 394–398, arXiv:1208.4563 [nucl-ex].
- [58] A. Bzdak and P. Bozek, “Contributions to the event-by-event charge asymmetry dependence for the elliptic flow of π^+ and π^- in heavy-ion collisions”, *Phys. Lett. B* **726** (2013) 239–243, arXiv:1303.1138 [nucl-th].
- [59] M. Stephanov and H.-U. Yee, “Charged elliptic flow at zero charge asymmetry”, *Phys. Rev. C* **88** (2013) 014908, arXiv:1304.6410 [nucl-th].
- [60] J. M. Campbell and M. A. Lisa, “Can baryon stopping explain the breakdown of constituent quark scaling and proposed signals of chiral magnetic waves at RHIC?”, *J. Phys. Conf. Ser.* **446** (2013) 012014.
- [61] S. A. Voloshin and R. Belmont, “Measuring and interpreting charge dependent anisotropic flow”, *Nucl. Phys. A* **931** (2014) 992–996, arXiv:1408.0714 [nucl-ex].
- [62] Y. Hatta, A. Monnai, and B.-W. Xiao, “Elliptic flow difference of charged pions in heavy-ion collisions”, *Nucl. Phys. A* **947** (2016) 155–160, arXiv:1507.04690 [hep-ph].
- [63] M. Hongo, Y. Hirono, and T. Hirano, “Anomalous-hydrodynamic analysis of charge-dependent elliptic flow in heavy-ion collisions”, *Phys. Lett. B* **775** (2017) 266–270, arXiv:1309.2823 [nucl-th].
- [64] X.-L. Zhao, G.-L. Ma, and Y.-G. Ma, “Novel mechanism for electric quadrupole moment generation in relativistic heavy-ion collisions”, *Phys. Lett. B* **792** (2019) 413–418, arXiv:1901.04156 [hep-ph].
- [65] H.-j. Xu, J. Zhao, Y. Feng, and F. Wang, “Complications in the interpretation of the charge asymmetry dependent π flow for the chiral magnetic wave”, *Phys. Rev. C* **101** (2020) 014913, arXiv:1910.02896 [nucl-th].
- [66] S. A. Bass, P. Danielewicz, and S. Pratt, “Clocking hadronization in relativistic heavy ion collisions with balance functions”, *Phys. Rev. Lett.* **85** (2000) 2689–2692, arXiv:nucl-th/0005044.
- [67] **ALICE** Collaboration, B. Abelev *et al.*, “Charge correlations using the balance function in Pb–Pb collisions at $\sqrt{s_{NN}} = 2.76$ TeV”, *Phys. Lett. B* **723** (2013) 267–279, arXiv:1301.3756 [nucl-ex].
- [68] W.-Y. Wu, C.-Z. Wang, Q.-Y. Shou, Y.-G. Ma, and L. Zheng, “Charge-dependent transverse momentum and its impact on the search for the chiral magnetic wave”, *Phys. Rev. C* **103** (2021) 034906, arXiv:2010.09955 [nucl-th].

- [69] G.-L. Ma, “Final state effects on charge asymmetry of pion elliptic flow in high-energy heavy-ion collisions”, *Phys. Lett. B* **735** (2014) 383–386, arXiv:1401.6502 [nucl-th].
- [70] W.-H. Zhou and J. Xu, “Simulating the Chiral Magnetic Wave in a Box System”, *Phys. Rev. C* **98** (2018) 044904, arXiv:1810.01030 [nucl-th].
- [71] Z.-Z. Han and J. Xu, “Charge asymmetry dependence of the elliptic flow splitting in relativistic heavy-ion collisions”, *Phys. Rev. C* **99** (2019) 044915, arXiv:1904.03544 [nucl-th].
- [72] D. Shen, J. Chen, G. Ma, Y.-G. Ma, Q. Shou, S. Zhang, and C. Zhong, “Charge asymmetry dependence of flow and a novel correlator to detect the chiral magnetic wave in a multiphase transport model”, *Phys. Rev. C* **100** (2019) 064907, arXiv:1911.00839 [hep-ph].
- [73] N. Magdy, M.-W. Nie, L. Huang, G.-L. Ma, and R. A. Lacey, “An extended $R_{\Psi_m}^{(2)}(\Delta S_2)$ correlator for detecting and characterizing the Chiral Magnetic Wave”, *Phys. Lett. B* **811** (2020) 135986, arXiv:2003.02396 [nucl-ex].
- [74] S. Shi, Y. Jiang, E. Lilleskov, and J. Liao, “Anomalous Chiral Transport in Heavy Ion Collisions from Anomalous-Viscous Fluid Dynamics”, *Annals Phys.* **394** (2018) 50–72, arXiv:1711.02496 [nucl-th].
- [75] W.-Y. Wu *et al.*, “Global constraint on the magnitude of anomalous chiral effects in heavy-ion collisions”, *Phys. Rev. C* **107** (2023) L031902, arXiv:2211.15446 [nucl-th].
- [76] ALICE Collaboration, K. Aamodt *et al.*, “The ALICE experiment at the CERN LHC”, *JINST* **3** (2008) S08002.
- [77] ALICE Collaboration, B. B. Abelev *et al.*, “Performance of the ALICE Experiment at the CERN LHC”, *Int. J. Mod. Phys. A* **29** (2014) 1430044, arXiv:1402.4476 [nucl-ex].
- [78] J. Alme *et al.*, “The ALICE TPC, a large 3-dimensional tracking device with fast readout for ultra-high multiplicity events”, *Nucl. Instrum. Meth. A* **622** (2010) 316–367, arXiv:1001.1950 [physics.ins-det].
- [79] ALICE Collaboration, G. Dellacasa *et al.*, “ALICE technical design report of the time-of-flight system (TOF)”, *CERN-LHCC-2000-012*.
- [80] ALICE Collaboration, E. Abbas *et al.*, “Performance of the ALICE VZERO system”, *JINST* **8** (2013) P10016, arXiv:1306.3130 [nucl-ex].
- [81] ALICE Collaboration, S. Acharya *et al.*, “Constraining the Chiral Magnetic Effect with charge-dependent azimuthal correlations in Pb–Pb collisions at $\sqrt{s_{NN}} = 2.76$ and 5.02 TeV”, *JHEP* **09** (2020) 160, arXiv:2005.14640 [nucl-ex].
- [82] ALICE Collaboration, B. Abelev *et al.*, “Centrality determination of Pb–Pb collisions at $\sqrt{s_{NN}} = 2.76$ TeV with ALICE”, *Phys. Rev. C* **88** (2013) 044909, arXiv:1301.4361 [nucl-ex].
- [83] M. Gyulassy and X.-N. Wang, “HIJING 1.0: A Monte Carlo program for parton and particle production in high-energy hadronic and nuclear collisions”, *Comput. Phys. Commun.* **83** (1994) 307, arXiv:nucl-th/9502021.
- [84] R. Brun, F. Bruyant, F. Carminati, S. Giani, M. Maire, A. McPherson, G. Patrick, and L. Urban, “GEANT Detector Description and Simulation Tool”, *CERN Program Library*, CERN, Geneva (1993).









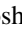
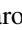
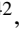








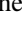
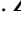




- [85] A. Bilandzic, R. Snellings, and S. Voloshin, “Flow analysis with cumulants: Direct calculations”, *Phys. Rev. C* **83** (2011) 044913, arXiv:1010.0233 [nucl-ex].
- [86] Y. Zhou, X. Zhu, P. Li, and H. Song, “Investigation of possible hadronic flow in $\sqrt{s_{NN}} = 5.02$ TeV $p - Pb$ collisions”, *Phys. Rev. C* **91** (2015) 064908, arXiv:1503.06986 [nucl-th].
- [87] R. Barlow, “Systematic errors: Facts and fictions”, in *Advanced Statistical Techniques in Particle Physics. Proceedings, Conference, Durham, UK, March 18-22, 2002*, pp. 134–144. 2002. arXiv:hep-ex/0207026 [hep-ex].
- [88] H.-j. Xu, J. Zhao, Y. Feng, and F. Wang, “Importance of non-flow background on the chiral magnetic wave search”, *Nucl. Phys. A* **1005** (2021) 121770, arXiv:2002.05220 [nucl-th].
- [89] ALICE Collaboration, J. Adam *et al.*, “Correlated event-by-event fluctuations of flow harmonics in Pb–Pb collisions at $\sqrt{s_{NN}} = 2.76$ TeV”, *Phys. Rev. Lett.* **117** (2016) 182301, arXiv:1604.07663 [nucl-ex].
- [90] ALICE Collaboration, K. Aamodt *et al.*, “Higher harmonic anisotropic flow measurements of charged particles in Pb–Pb collisions at $\sqrt{s_{NN}}=2.76$ TeV”, *Phys. Rev. Lett.* **107** (2011) 032301, arXiv:1105.3865 [nucl-ex].
- [91] ATLAS Collaboration, G. Aad *et al.*, “Measurement of event-plane correlations in $\sqrt{s_{NN}} = 2.76$ TeV lead-lead collisions with the ATLAS detector”, *Phys. Rev. C* **90** (2014) 024905, arXiv:1403.0489 [hep-ex].
- [92] Y. Hatta, “Analytic approaches to relativistic hydrodynamics”, *Nucl. Phys. A* **956** (2016) 152–159, arXiv:1601.04128 [hep-ph].

A The ALICE Collaboration

S. Acharya ¹²⁸, D. Adamová ⁸⁷, G. Aglieri Rinella ³³, M. Agnello ³⁰, N. Agrawal ⁵², Z. Ahammed ¹³⁶, S. Ahmad ¹⁶, S.U. Ahn ⁷², I. Ahuja ³⁸, A. Akhmedov ¹⁴², M. Al-Turany ⁹⁸, D. Aleksandrov ¹⁴², B. Alessandro ⁵⁷, H.M. Alfanda ⁶, R. Alfaro Molina ⁶⁸, B. Ali ¹⁶, A. Alici ²⁶, N. Alizadehvandchali ¹¹⁷, A. Alkin ³³, J. Alme ²¹, G. Alocco ⁵³, T. Alt ⁶⁵, A.R. Altamura ⁵¹, I. Altsybeev ⁹⁶, J.R. Alvarado ⁴⁵, M.N. Anaam ⁶, C. Andrei ⁴⁶, N. Andreou ¹¹⁶, A. Andronic ¹²⁷, V. Anguelov ⁹⁵, F. Antinori ⁵⁵, P. Antonioli ⁵², N. Apadula ⁷⁵, L. Aphecetche ¹⁰⁴, H. Appelshäuser ⁶⁵, C. Arata ⁷⁴, S. Arce ²⁶, M. Aresti ²³, R. Arnaldi ⁵⁷, J.G.M.C.A. Arneiro ¹¹¹, I.C. Arsene ²⁰, M. Arslandok ¹³⁹, A. Augustinus ³³, R. Averbeck ⁹⁸, M.D. Azmi ¹⁶, H. Baba ¹²⁵, A. Badalà ⁵⁴, J. Bae ¹⁰⁵, Y.W. Baek ⁴¹, X. Bai ¹²¹, R. Bailhache ⁶⁵, Y. Bailung ⁴⁹, A. Balbino ³⁰, A. Baldisseri ¹³¹, B. Balis ², D. Banerjee ⁴, Z. Banoo ⁹², R. Barbera ²⁷, F. Barile ³², L. Barioglio ⁹⁶, M. Barlou ⁷⁹, B. Barman ⁴², G.G. Barnaföldi ⁴⁷, L.S. Barnby ⁸⁶, V. Barret ¹²⁸, L. Barreto ¹¹¹, C. Bartels ¹²⁰, K. Barth ³³, E. Bartsch ⁶⁵, N. Bastid ¹²⁸, S. Basu ⁷⁶, G. Batigne ¹⁰⁴, D. Battistini ⁹⁶, B. Batyunya ¹⁴³, D. Bauri ⁴⁸, J.L. Bazo Alba ¹⁰², I.G. Bearden ⁸⁴, C. Beattie ¹³⁹, P. Becht ⁹⁸, D. Behera ⁴⁹, I. Belikov ¹³⁰, A.D.C. Bell Hechavarria ¹²⁷, F. Bellini ²⁶, R. Bellwied ¹¹⁷, S. Belokurova ¹⁴², Y.A.V. Beltran ⁴⁵, G. Bencedi ⁴⁷, S. Beole ²⁵, Y. Berdnikov ¹⁴², A. Berdnikova ⁹⁵, L. Bergmann ⁹⁵, M.G. Besoiu ⁶⁴, L. Betev ³³, P.P. Bhaduri ¹³⁶, A. Bhasin ⁹², M.A. Bhat ⁴, B. Bhattacharjee ⁴², L. Bianchi ²⁵, N. Bianchi ⁵⁰, J. Bielčík ³⁶, J. Bielčíková ⁸⁷, J. Biernat ¹⁰⁸, A.P. Bigot ¹³⁰, A. Bilandzic ⁹⁶, G. Biro ⁴⁷, S. Biswas ⁴, N. Bize ¹⁰⁴, J.T. Blair ¹⁰⁹, D. Blau ¹⁴², M.B. Blidaru ⁹⁸, N. Bluhme ³⁹, C. Blume ⁶⁵, G. Boca ^{22,56}, F. Bock ⁸⁸, T. Bodova ²¹, A. Bogdanov ¹⁴², S. Boi ²³, J. Bok ⁵⁹, L. Boldizsár ⁴⁷, M. Bombara ³⁸, P.M. Bond ³³, G. Bonomi ^{135,56}, H. Borel ¹³¹, A. Borissov ¹⁴², A.G. Borquez Carcamo ⁹⁵, H. Bossi ¹³⁹, E. Botta ²⁵, Y.E.M. Bouziani ⁶⁵, L. Bratrud ⁶⁵, P. Braun-Munzinger ⁹⁸, M. Bregant ¹¹¹, M. Broz ³⁶, G.E. Bruno ^{97,32}, M.D. Buckland ²⁴, D. Budnikov ¹⁴², H. Buesching ⁶⁵, S. Bufalino ³⁰, P. Buhler ¹⁰³, N. Burmasov ¹⁴², Z. Buthelezi ^{69,124}, A. Bylinkin ²¹, S.A. Bysiak ¹⁰⁸, M. Cai ⁶, H. Caines ¹³⁹, A. Caliva ²⁹, E. Calvo Villar ¹⁰², J.M.M. Camacho ¹¹⁰, P. Camerini ²⁴, F.D.M. Canedo ¹¹¹, S.L. Cantway ¹³⁹, M. Carabas ¹¹⁴, A.A. Carballo ³³, F. Carnesecchi ³³, R. Caron ¹²⁹, L.A.D. Carvalho ¹¹¹, J. Castillo Castellanos ¹³¹, F. Catalano ^{33,25}, C. Ceballos Sanchez ¹⁴³, I. Chakaberia ⁷⁵, P. Chakraborty ⁴⁸, S. Chandra ¹³⁶, S. Chapeland ³³, M. Chartier ¹²⁰, S. Chattopadhyay ¹³⁶, S. Chattopadhyay ¹⁰⁰, T. Cheng ^{98,6}, C. Cheshkov ¹²⁹, B. Cheynis ¹²⁹, V. Chibante Barroso ³³, D.D. Chinellato ¹¹², E.S. Chizzali ^{11,96}, J. Cho ⁵⁹, S. Cho ⁵⁹, P. Chochula ³³, D. Choudhury ⁴², P. Christakoglou ⁸⁵, C.H. Christensen ⁸⁴, P. Christiansen ⁷⁶, T. Chujo ¹²⁶, M. Ciaccio ³⁰, C. Cicalo ⁵³, F. Cindolo ⁵², M.R. Ciupek ⁹⁸, G. Clai ^{III,52}, F. Colamaria ⁵¹, J.S. Colburn ¹⁰¹, D. Colella ^{97,32}, M. Colocci ²⁶, M. Concas ^{IV,33}, G. Conesa Balbastre ⁷⁴, Z. Conesa del Valle ¹³², G. Contin ²⁴, J.G. Contreras ³⁶, M.L. Coquet ¹³¹, P. Cortese ^{134,57}, M.R. Cosentino ¹¹³, F. Costa ³³, S. Costanza ^{22,56}, C. Cot ¹³², J. Crkovská ⁹⁵, P. Crochet ¹²⁸, R. Cruz-Torres ⁷⁵, P. Cui ⁶, A. Dainese ⁵⁵, M.C. Danisch ⁹⁵, A. Danu ⁶⁴, P. Das ⁸¹, P. Das ⁴, S. Das ⁴, A.R. Dash ¹²⁷, S. Dash ⁴⁸, A. De Caro ²⁹, G. de Cataldo ⁵¹, J. de Cuveland ³⁹, A. De Falco ²³, D. De Gruttola ²⁹, N. De Marco ⁵⁷, C. De Martin ²⁴, S. De Pasquale ²⁹, R. Deb ¹³⁵, R. Del Grande ⁹⁶, L. Dello Stritto ²⁹, W. Deng ⁶, P. Dhankher ¹⁹, D. Di Bari ³², A. Di Mauro ³³, B. Diab ¹³¹, R.A. Diaz ^{143,7}, T. Dietel ¹¹⁵, Y. Ding ⁶, J. Ditzel ⁶⁵, R. Divià ³³, D.U. Dixit ¹⁹, Ø. Djuvland ²¹, U. Dmitrieva ¹⁴², A. Dobrin ⁶⁴, B. Dönigus ⁶⁵, J.M. Dubinski ¹³⁷, A. Dubla ⁹⁸, S. Dudi ⁹¹, P. Dupieux ¹²⁸, M. Durkac ¹⁰⁷, N. Dzalaiova ¹³, T.M. Eder ¹²⁷, R.J. Ehlers ⁷⁵, F. Eisenhut ⁶⁵, R. Ejima ⁹³, D. Elia ⁵¹, B. Erazmus ¹⁰⁴, F. Ercolessi ²⁶, B. Espagnon ¹³², G. Eulisse ³³, D. Evans ¹⁰¹, S. Evdokimov ¹⁴², L. Fabbietti ⁹⁶, M. Faggin ²⁸, J. Faivre ⁷⁴, F. Fan ⁶, W. Fan ⁷⁵, A. Fantoni ⁵⁰, M. Fasel ⁸⁸, A. Feliciello ⁵⁷, G. Feofilov ¹⁴², A. Fernández Téllez ⁴⁵, L. Ferrandi ¹¹¹, M.B. Ferrer ³³, A. Ferrero ¹³¹, C. Ferrero ⁵⁷, A. Ferretti ²⁵, V.J.G. Feuillard ⁹⁵, V. Filova ³⁶, D. Finogeev ¹⁴², F.M. Fionda ⁵³, E. Flatland ³³, F. Flor ¹¹⁷, A.N. Flores ¹⁰⁹, S. Foertsch ⁶⁹, I. Fokin ⁹⁵, S. Fokin ¹⁴², E. Fragiaco ⁵⁸, E. Frajna ⁴⁷, U. Fuchs ³³, N. Funicello ²⁹, C. Furget ⁷⁴, A. Furs ¹⁴², T. Fusayasu ⁹⁹, J.J. Gaardhøje ⁸⁴, M. Gagliardi ²⁵, A.M. Gago ¹⁰², T. Gahlaut ⁴⁸, C.D. Galvan ¹¹⁰, D.R. Gangadharan ¹¹⁷, P. Ganoti ⁷⁹, C. Garabatos ⁹⁸, A.T. Garcia ¹³², T. García Chávez ⁴⁵, E. Garcia-Solis ⁹, C. Gargiulo ³³, P. Gasik ⁹⁸, A. Gautam ¹¹⁹, M.B. Gay Ducati ⁶⁷, M. Germain ¹⁰⁴, A. Ghimouz ¹²⁶, C. Ghosh ¹³⁶, M. Giacalone ⁵², G. Gioachin ³⁰, P. Giubellino ^{98,57}, P. Giubileo ²⁸, A.M.C. Glaenzer ¹³¹, P. Glässel ⁹⁵, E. Glimos ¹²³, D.J.Q. Goh ⁷⁷, V. Gonzalez ¹³⁸, P. Gordeev ¹⁴², M. Gorgon ², K. Goswami ⁴⁹, S. Gotovac ³⁴, V. Grabski ⁶⁸, L.K. Graczykowski ¹³⁷, E. Grecka ⁸⁷, A. Grelli ⁶⁰, C. Grigoras ³³, V. Grigoriev ¹⁴², S. Grigoryan ^{143,1}, F. Grosa ³³, J.F. Grosse-Oetringhaus ³³, R. Grosso ⁹⁸, D. Grund ³⁶, N.A. Grunwald ⁹⁵, G.G. Guardiano ¹¹², R. Guernane ⁷⁴, M. Guilbaud ¹⁰⁴,

K. Gulbrandsen ⁸⁴, T. Gündem ⁶⁵, T. Gunji ¹²⁵, W. Guo ⁶, A. Gupta ⁹², R. Gupta ⁹², R. Gupta ⁴⁹,
 K. Gwizdziel ¹³⁷, L. Gyulai ⁴⁷, C. Hadjidakis ¹³², F.U. Haider ⁹², S. Haidlova ³⁶, H. Hamagaki ⁷⁷,
 A. Hamdi ⁷⁵, Y. Han ¹⁴⁰, B.G. Hanley ¹³⁸, R. Hannigan ¹⁰⁹, J. Hansen ⁷⁶, M.R. Haque ¹³⁷,
 J.W. Harris ¹³⁹, A. Harton ⁹, H. Hassan ¹¹⁸, D. Hatzifotiadou ⁵², P. Hauer ⁴³, L.B. Havener ¹³⁹,
 S.T. Heckel ⁹⁶, E. Hellbär ⁹⁸, H. Helstrup ³⁵, M. Hemmer ⁶⁵, T. Herman ³⁶, G. Herrera Corral ⁸,
 F. Herrmann ¹²⁷, S. Herrmann ¹²⁹, K.F. Hetland ³⁵, B. Heybeck ⁶⁵, H. Hillemanns ³³, B. Hippolyte ¹³⁰,
 F.W. Hoffmann ⁷¹, B. Hofman ⁶⁰, G.H. Hong ¹⁴⁰, M. Horst ⁹⁶, A. Horzyk ², Y. Hou ⁶, P. Hristov ³³,
 C. Hughes ¹²³, P. Huhn ⁶⁵, L.M. Huhta ¹¹⁸, T.J. Humanic ⁸⁹, A. Hutson ¹¹⁷, D. Hutter ³⁹, R. Ilkaev ¹⁴²,
 H. Ilyas ¹⁴, M. Inaba ¹²⁶, G.M. Innocenti ³³, M. Ippolitov ¹⁴², A. Isakov ^{85,87}, T. Isidori ¹¹⁹,
 M.S. Islam ¹⁰⁰, M. Ivanov ¹³, M. Ivanov ⁹⁸, V. Ivanov ¹⁴², K.E. Iversen ⁷⁶, M. Jablonski ², B. Jacak ⁷⁵,
 N. Jacazio ²⁶, P.M. Jacobs ⁷⁵, S. Jadlovská ¹⁰⁷, J. Jadlovsky ¹⁰⁷, S. Jaelani ⁸³, C. Jahnke ¹¹¹,
 M.J. Jakubowska ¹³⁷, M.A. Janik ¹³⁷, T. Janson ⁷¹, S. Ji ¹⁷, S. Jia ¹⁰, A.A.P. Jimenez ⁶⁶, F. Jonas ^{88,127},
 D.M. Jones ¹²⁰, J.M. Jowett ^{33,98}, J. Jung ⁶⁵, M. Jung ⁶⁵, A. Junique ³³, A. Jusko ¹⁰¹,
 M.J. Kabus ^{33,137}, J. Kaewjai ¹⁰⁶, P. Kalinak ⁶¹, A.S. Kalteyer ⁹⁸, A. Kalweit ³³, V. Kaplin ¹⁴², A. Karasu
 Uysal ⁷³, D. Karatovic ⁹⁰, O. Karavichev ¹⁴², T. Karavicheva ¹⁴², P. Karczmarczyk ¹³⁷,
 E. Karpechev ¹⁴², U. Kebschull ⁷¹, R. Keidel ¹⁴¹, D.L.D. Keijdener ⁶⁰, M. Keil ³³, B. Ketzer ⁴³,
 S.S. Khade ⁴⁹, A.M. Khan ¹²¹, S. Khan ¹⁶, A. Khanzadeev ¹⁴², Y. Kharlov ¹⁴², A. Khatun ¹¹⁹,
 A. Khuntia ³⁶, B. Kileng ³⁵, B. Kim ¹⁰⁵, C. Kim ¹⁷, D.J. Kim ¹¹⁸, E.J. Kim ⁷⁰, J. Kim ¹⁴⁰,
 J.S. Kim ⁴¹, J. Kim ⁵⁹, J. Kim ⁷⁰, M. Kim ¹⁹, S. Kim ¹⁸, T. Kim ¹⁴⁰, K. Kimura ⁹³, S. Kirsch ⁶⁵,
 I. Kisel ³⁹, S. Kiselev ¹⁴², A. Kisiel ¹³⁷, J.P. Kitowski ², J.L. Klay ⁵, J. Klein ³³, S. Klein ⁷⁵,
 C. Klein-Bösing ¹²⁷, M. Kleiner ⁶⁵, T. Klemenz ⁹⁶, A. Kluge ³³, A.G. Knospe ¹¹⁷, C. Kobdaj ¹⁰⁶,
 T. Kollegger ⁹⁸, A. Kondratyev ¹⁴³, N. Kondratyeva ¹⁴², E. Kondratyuk ¹⁴², J. König ⁶⁵,
 S.A. Königstorfer ⁹⁶, P.J. Konopka ³³, G. Kornakov ¹³⁷, M. Korwieser ⁹⁶, S.D. Koryciak ²,
 A. Kotliarov ⁸⁷, V. Kovalenko ¹⁴², M. Kowalski ¹⁰⁸, V. Kozhuharov ³⁷, I. Králik ⁶¹, A. Kravčáková ³⁸,
 L. Krcal ^{33,39}, M. Krivda ^{101,61}, F. Krizek ⁸⁷, K. Krizkova Gajdosova ³³, M. Kroesen ⁹⁵, M. Krüger ⁶⁵,
 D.M. Krupova ³⁶, E. Kryshen ¹⁴², V. Kučera ⁵⁹, C. Kuhn ¹³⁰, P.G. Kuijer ⁸⁵, T. Kumaoka ¹²⁶,
 D. Kumar ¹³⁶, L. Kumar ⁹¹, N. Kumar ⁹¹, S. Kumar ³², S. Kundu ³³, P. Kurashvili ⁸⁰, A. Kurepin ¹⁴²,
 A.B. Kurepin ¹⁴², A. Kuryakin ¹⁴², S. Kushpil ⁸⁷, V. Kuskov ¹⁴², M.J. Kweon ⁵⁹, Y. Kwon ¹⁴⁰, S.L. La
 Pointe ³⁹, P. La Rocca ²⁷, A. Lakrathok ¹⁰⁶, M. Lamanna ³³, A.R. Landou ^{74,116}, R. Langoy ¹²²,
 P. Larionov ³³, E. Laudi ³³, L. Lautner ^{33,96}, R. Lavicka ¹⁰³, R. Lea ^{135,56}, H. Lee ¹⁰⁵, I. Legrand ⁴⁶,
 G. Legras ¹²⁷, J. Lehrbach ³⁹, T.M. Lelek ², R.C. Lemmon ⁸⁶, I. León Monzón ¹¹⁰, M.M. Lesch ⁹⁶,
 E.D. Lesser ¹⁹, P. Lévai ⁴⁷, X. Li ¹⁰, J. Lien ¹²², R. Lietava ¹⁰¹, I. Likmeta ¹¹⁷, B. Lim ²⁵, S.H. Lim ¹⁷,
 V. Lindenstruth ³⁹, A. Lindner ⁴⁶, C. Lippmann ⁹⁸, D.H. Liu ⁶, J. Liu ¹²⁰, G.S.S. Liveraro ¹¹²,
 I.M. Lofnes ²¹, C. Loizides ⁸⁸, S. Lokos ¹⁰⁸, J. Lomker ⁶⁰, P. Loncar ³⁴, X. Lopez ¹²⁸, E. López
 Torres ⁷, P. Lu ^{98,121}, F.V. Lugo ⁶⁸, J.R. Lühder ¹²⁷, M. Lunardon ²⁸, G. Luparello ⁵⁸, Y.G. Ma ⁴⁰,
 M. Mager ³³, A. Maire ¹³⁰, E.M. Majerz ², M.V. Makariev ³⁷, M. Malaev ¹⁴², G. Malfattore ²⁶,
 N.M. Malik ⁹², Q.W. Malik ²⁰, S.K. Malik ⁹², L. Malinina ^{I,VII,143}, D. Mallick ^{132,81}, N. Mallick ⁴⁹,
 G. Mandaglio ^{31,54}, S.K. Mandal ⁸⁰, V. Manko ¹⁴², F. Manso ¹²⁸, V. Manzari ⁵¹, Y. Mao ⁶,
 R.W. Marcjan ², G.V. Margagliotti ²⁴, A. Margotti ⁵², A. Marín ⁹⁸, C. Markert ¹⁰⁹, P. Martinengo ³³,
 M.I. Martínez ⁴⁵, G. Martínez García ¹⁰⁴, M.P.P. Martins ¹¹¹, S. Masciocchi ⁹⁸, M. Masera ²⁵,
 A. Masoni ⁵³, L. Massacrier ¹³², O. Massen ⁶⁰, A. Mastroserio ^{133,51}, O. Matonoha ⁷⁶, S. Mattiazzo ²⁸,
 A. Matyja ¹⁰⁸, C. Mayer ¹⁰⁸, A.L. Mazuecos ³³, F. Mazzaschi ²⁵, M. Mazzilli ³³, J.E. Mdhuli ¹²⁴,
 Y. Melikyan ⁴⁴, A. Menchaca-Rocha ⁶⁸, J.E.M. Mendez ⁶⁶, E. Meninno ¹⁰³, A.S. Menon ¹¹⁷,
 M. Meres ¹³, S. Mhlanga ^{115,69}, Y. Miake ¹²⁶, L. Micheletti ³³, D.L. Mihaylov ⁹⁶, K. Mikhaylov ^{143,142},
 A.N. Mishra ⁴⁷, D. Miśkowiec ⁹⁸, A. Modak ⁴, B. Mohanty ⁸¹, M. Mohisin Khan ^{V,16},
 M.A. Molander ⁴⁴, S. Monira ¹³⁷, C. Mordasini ¹¹⁸, D.A. Moreira De Godoy ¹²⁷, I. Morozov ¹⁴²,
 A. Morsch ³³, T. Mrnjavac ³³, V. Muccifora ⁵⁰, S. Muhuri ¹³⁶, J.D. Mulligan ⁷⁵, A. Mulliri ²³,
 M.G. Munhoz ¹¹¹, R.H. Munzer ⁶⁵, H. Murakami ¹²⁵, S. Murray ¹¹⁵, L. Musa ³³, J. Musinsky ⁶¹,
 J.W. Myrcha ¹³⁷, B. Naik ¹²⁴, A.I. Nambrath ¹⁹, B.K. Nandi ⁴⁸, R. Nania ⁵², E. Nappi ⁵¹,
 A.F. Nassirpour ¹⁸, A. Nath ⁹⁵, C. Nattrass ¹²³, M.N. Naydenov ³⁷, A. Neagu ²⁰, A. Negru ¹¹⁴,
 E. Nekrasova ¹⁴², L. Nellen ⁶⁶, R. Nepeivoda ⁷⁶, S. Nese ²⁰, G. Neskovic ³⁹, N. Nicassio ⁵¹,
 B.S. Nielsen ⁸⁴, E.G. Nielsen ⁸⁴, S. Nikolaev ¹⁴², S. Nikulin ¹⁴², V. Nikulin ¹⁴², F. Noferini ⁵²,
 S. Noh ¹², P. Nomokonov ¹⁴³, J. Norman ¹²⁰, N. Novitzky ⁸⁸, P. Nowakowski ¹³⁷, A. Nyanin ¹⁴²,
 J. Nystrand ²¹, M. Ogino ⁷⁷, S. Oh ¹⁸, A. Ohlson ⁷⁶, V.A. Okorokov ¹⁴², J. Oleniacz ¹³⁷, A.C. Oliveira
 Da Silva ¹²³, A. Onnerstad ¹¹⁸, C. Oppedisano ⁵⁷, A. Ortiz Velasquez ⁶⁶, J. Otwinowski ¹⁰⁸, M. Oya ⁹³,
 K. Oyama ⁷⁷, Y. Pachmayer ⁹⁵, S. Padhan ⁴⁸, D. Pagano ^{135,56}, G. Paic ⁶⁶, S. Paisano-Guzmán ⁴⁵,

A. Palasciano⁵¹, S. Panebianco¹³¹, H. Park¹²⁶, H. Park¹⁰⁵, J. Park⁵⁹, J.E. Parkkila³³, Y. Patley⁴⁸, R.N. Patra⁹², B. Paul²³, H. Pei⁶, T. Peitzmann⁶⁰, X. Peng¹¹, M. Pennisi²⁵, S. Perciballi²⁵, D. Peresunko¹⁴², G.M. Perez⁷, Y. Pestov¹⁴², V. Petrov¹⁴², M. Petrovici⁴⁶, R.P. Pezzi^{104,67}, S. Piano⁵⁸, M. Pikna¹³, P. Pillot¹⁰⁴, O. Pinazza^{52,33}, L. Pinsky¹¹⁷, C. Pinto⁹⁶, S. Pisano⁵⁰, M. Płoskoń⁷⁵, M. Planinic⁹⁰, F. Pliquett⁶⁵, M.G. Poghosyan⁸⁸, B. Polichtchouk¹⁴², S. Politano³⁰, N. Poljak⁹⁰, A. Pop⁴⁶, S. Porteboeuf-Houssais¹²⁸, V. Pozdniakov¹⁴³, I.Y. Pozos⁴⁵, K.K. Pradhan⁴⁹, S.K. Prasad⁴, S. Prasad⁴⁹, R. Preghenella⁵², F. Prino⁵⁷, C.A. Pruneau¹³⁸, I. Pshenichnov¹⁴², M. Puccio³³, S. Pucillo²⁵, Z. Pugelova¹⁰⁷, S. Qiu⁸⁵, L. Quaglia²⁵, S. Ragoni¹⁵, A. Rai¹³⁹, A. Rakotozafindrabe¹³¹, L. Ramello^{134,57}, F. Rami¹³⁰, T.A. Rancien⁷⁴, M. Rasa²⁷, S.S. Räsänen⁴⁴, R. Rath⁵², M.P. Rauch²¹, I. Ravasenga⁸⁵, K.F. Read^{88,123}, C. Reckziegel¹¹³, A.R. Redelbach³⁹, K. Redlich^{VI,80}, C.A. Retz⁹⁸, H.D. Regules-Medel⁴⁵, A. Rehman²¹, F. Reidt³³, H.A. Reme-Ness³⁵, Z. Rescakova³⁸, K. Reygers⁹⁵, A. Riabov¹⁴², V. Riabov¹⁴², R. Ricci²⁹, M. Richter²⁰, A.A. Riedel⁹⁶, W. Riegler³³, A.G. Riffero²⁵, C. Ristea⁶⁴, M.V. Rodriguez³³, M. Rodríguez Cahuantzi⁴⁵, S.A. Rodríguez Ramírez⁴⁵, K. Røed²⁰, R. Rogalev¹⁴², E. Rogochaya¹⁴³, T.S. Rogoschinski⁶⁵, D. Rohr³³, D. Röhrich²¹, P.F. Rojas⁴⁵, S. Rojas Torres³⁶, P.S. Rokita¹³⁷, G. Romanenko²⁶, F. Ronchetti⁵⁰, A. Rosano^{31,54}, E.D. Rosas⁶⁶, K. Roslon¹³⁷, A. Rossi⁵⁵, A. Roy⁴⁹, S. Roy⁴⁸, N. Rubini²⁶, D. Ruggiano¹³⁷, R. Rui²⁴, P.G. Russek², R. Russo⁸⁵, A. Rustamov⁸², E. Ryabinkin¹⁴², Y. Ryabov¹⁴², A. Rybicki¹⁰⁸, H. Rytönen¹¹⁸, J. Ryu¹⁷, W. Rzesza¹³⁷, O.A.M. Saariimaki⁴⁴, S. Sadhu³², S. Sadovsky¹⁴², J. Saetre²¹, K. Šafařík³⁶, P. Saha⁴², S.K. Saha⁴, S. Saha⁸¹, B. Sahoo⁴⁸, B. Sahoo⁴⁹, R. Sahoo⁴⁹, S. Sahoo⁶², D. Sahu⁴⁹, P.K. Sahu⁶², J. Saini¹³⁶, K. Sajdakova³⁸, S. Sakai¹²⁶, M.P. Salvan⁹⁸, S. Sambyal⁹², D. Samitz¹⁰³, I. Sanna^{33,96}, T.B. Saramela¹¹¹, P. Sarma⁴², V. Sarritzu²³, V.M. Sarti⁹⁶, M.H.P. Sas³³, S. Sawan⁸¹, J. Schambach⁸⁸, H.S. Scheid⁶⁵, C. Schiaua⁴⁶, R. Schicker⁹⁵, F. Schlepfer⁹⁵, A. Schmah⁹⁸, C. Schmidt⁹⁸, H.R. Schmidt⁹⁴, M.O. Schmidt³³, M. Schmidt⁹⁴, N.V. Schmidt⁸⁸, A.R. Schmier¹²³, R. Schotter¹³⁰, A. Schröter³⁹, J. Schukraft³³, K. Schweda⁹⁸, G. Scioli²⁶, E. Scomparin⁵⁷, J.E. Seger¹⁵, Y. Sekiguchi¹²⁵, D. Sekihata¹²⁵, M. Selina⁸⁵, I. Selyuzhenkov⁹⁸, S. Senyukov¹³⁰, J.J. Seo^{95,59}, D. Serebryakov¹⁴², L. Šerkšnytė⁹⁶, A. Sevcenco⁶⁴, T.J. Shaba⁶⁹, A. Shabetai¹⁰⁴, R. Shahoyan³³, A. Shangaraev¹⁴², A. Sharma⁹¹, B. Sharma⁹², D. Sharma⁴⁸, H. Sharma⁵⁵, M. Sharma⁹², S. Sharma⁷⁷, S. Sharma⁹², U. Sharma⁹², A. Shatat¹³², O. Sheibani¹¹⁷, K. Shigaki⁹³, M. Shimomura⁷⁸, J. Shin¹², S. Shirinkin¹⁴², Q. Shou⁴⁰, Y. Sibirak¹⁴², S. Siddhanta⁵³, T. Siemiarczuk⁸⁰, T.F. Silva¹¹¹, D. Silvermyr⁷⁶, T. Simantathammakul¹⁰⁶, R. Simeonov³⁷, B. Singh⁹², B. Singh⁹⁶, K. Singh⁴⁹, R. Singh⁸¹, R. Singh⁹², R. Singh⁴⁹, S. Singh¹⁶, V.K. Singh¹³⁶, V. Singhal¹³⁶, T. Sinha¹⁰⁰, B. Sitar¹³, M. Sitta^{134,57}, T.B. Skaali²⁰, G. Skorodumovs⁹⁵, M. Slupecki⁴⁴, N. Smirnov¹³⁹, R.J.M. Snellings⁶⁰, E.H. Solheim²⁰, J. Song¹⁷, C. Sonnabend^{33,98}, F. Soramel²⁸, A.B. Soto-hernandez⁸⁹, R. Spijkers⁸⁵, I. Sputowska¹⁰⁸, J. Staa⁷⁶, J. Stachel⁹⁵, I. Stan⁶⁴, P.J. Steffanic¹²³, S.F. Stiefelmaier⁹⁵, D. Stocco¹⁰⁴, I. Storehaug²⁰, P. Stratmann¹²⁷, S. Strazzi²⁶, A. Sturniolo^{31,54}, C.P. Stylianidis⁸⁵, A.A.P. Suaide¹¹¹, C. Suire¹³², M. Sukhanov¹⁴², M. Suljic³³, R. Sultanov¹⁴², V. Sumberia⁹², S. Sumowidagdo⁸³, S. Swain⁶², I. Szarka¹³, M. Szymkowski¹³⁷, S.F. Taghavi⁹⁶, G. Taillepied⁹⁸, J. Takahashi¹¹², G.J. Tambave⁸¹, S. Tang⁶, Z. Tang¹²¹, J.D. Tapia Takaki¹¹⁹, N. Tapus¹¹⁴, L.A. Tarasovicova¹²⁷, M.G. Tarzila⁴⁶, G.F. Tassielli³², A. Tauro³³, G. Tejada Muñoz⁴⁵, A. Telesca³³, L. Terlizzi²⁵, C. Terrevoli¹¹⁷, S. Thakur⁴, D. Thomas¹⁰⁹, A. Tikhonov¹⁴², N. Tiltmann¹²⁷, A.R. Timmins¹¹⁷, M. Tkacik¹⁰⁷, T. Tkacik¹⁰⁷, A. Toia⁶⁵, R. Tokumoto⁹³, K. Tomohiro⁹³, N. Topilskaya¹⁴², M. Toppi⁵⁰, T. Tork¹³², P.V. Torres⁶⁶, V.V. Torres¹⁰⁴, A.G. Torres Ramos³², A. Trifiro^{31,54}, A.S. Triolo^{33,31,54}, S. Tripathy⁵², T. Tripathy⁴⁸, S. Trogolo³³, V. Trubnikov³, W.H. Trzaska¹¹⁸, T.P. Trzcinski¹³⁷, A. Tumkin¹⁴², R. Turrisi⁵⁵, T.S. Tveter²⁰, K. Ullaland²¹, B. Ulukutlu⁹⁶, A. Uras¹²⁹, G.L. Usai²³, M. Vala³⁸, N. Valle²², L.V.R. van Doremalen⁶⁰, M. van Leeuwen⁸⁵, C.A. van Veen⁹⁵, R.J.G. van Weelden⁸⁵, P. Vande Vyvre³³, D. Varga⁴⁷, Z. Varga⁴⁷, M. Vasileiou⁷⁹, A. Vasiliev¹⁴², O. Vázquez Doce⁵⁰, O. Vazquez Rueda¹¹⁷, V. Vechernin¹⁴², E. Vercellin²⁵, S. Vergara Limón⁴⁵, R. Verma⁴⁸, L. Vermunt⁹⁸, R. Vértesi⁴⁷, M. Verweij⁶⁰, L. Vickovic³⁴, Z. Vilakazi¹²⁴, O. Villalobos Baillie¹⁰¹, A. Villani²⁴, A. Vinogradov¹⁴², T. Virgili²⁹, M.M.O. Virta¹¹⁸, V. Vislavicius⁷⁶, A. Vodopyanov¹⁴³, B. Volkel³³, M.A. Völkl⁹⁵, K. Voloshin¹⁴², S.A. Voloshin¹³⁸, G. Volpe³², B. von Haller³³, I. Vorobyev⁹⁶, N. Vozniuk¹⁴², J. Vrláková³⁸, J. Wan⁴⁰, C. Wang⁴⁰, D. Wang⁴⁰, Y. Wang⁴⁰, Y. Wang⁶, A. Wegrzynek³³, F.T. Weiglhofer³⁹, S.C. Wenzel³³, J.P. Wessels¹²⁷, J. Wiechula⁶⁵, J. Wikne²⁰, G. Wilk⁸⁰, J. Wilkinson⁹⁸, G.A. Willems¹²⁷, B. Windelband⁹⁵, M. Winn¹³¹, J.R. Wright¹⁰⁹, W. Wu⁴⁰, Y. Wu¹²¹, R. Xu⁶, A. Yadav⁴³, A.K. Yadav¹³⁶, S. Yalcin⁷³, Y. Yamaguchi⁹³, S. Yang²¹,

S. Yano ⁹³, Z. Yin ⁶, I.-K. Yoo ¹⁷, J.H. Yoon ⁵⁹, H. Yu¹², S. Yuan²¹, A. Yuncu ⁹⁵, V. Zaccolo ²⁴, C. Zampolli ³³, F. Zanone ⁹⁵, N. Zardoshti ³³, A. Zarochentsev ¹⁴², P. Závada ⁶³, N. Zaviyalov¹⁴², M. Zhalov ¹⁴², B. Zhang ⁶, C. Zhang ¹³¹, L. Zhang ⁴⁰, S. Zhang ⁴⁰, X. Zhang ⁶, Y. Zhang¹²¹, Z. Zhang ⁶, M. Zhao ¹⁰, V. Zherebchevskii ¹⁴², Y. Zhi¹⁰, D. Zhou ⁶, Y. Zhou ⁸⁴, J. Zhu ^{98,6}, Y. Zhu⁶, S.C. Zugeravel ⁵⁷, N. Zurlo ^{135,56}

Affiliation Notes

^I Deceased

^{II} Also at: Max-Planck-Institut für Physik, Munich, Germany

^{III} Also at: Italian National Agency for New Technologies, Energy and Sustainable Economic Development (ENEA), Bologna, Italy

^{IV} Also at: Dipartimento DET del Politecnico di Torino, Turin, Italy

^V Also at: Department of Applied Physics, Aligarh Muslim University, Aligarh, India

^{VI} Also at: Institute of Theoretical Physics, University of Wrocław, Poland

^{VII} Also at: An institution covered by a cooperation agreement with CERN

Collaboration Institutes

¹ A.I. Alikhanyan National Science Laboratory (Yerevan Physics Institute) Foundation, Yerevan, Armenia

² AGH University of Krakow, Cracow, Poland

³ Bogolyubov Institute for Theoretical Physics, National Academy of Sciences of Ukraine, Kiev, Ukraine

⁴ Bose Institute, Department of Physics and Centre for Astroparticle Physics and Space Science (CAPSS), Kolkata, India

⁵ California Polytechnic State University, San Luis Obispo, California, United States

⁶ Central China Normal University, Wuhan, China

⁷ Centro de Aplicaciones Tecnológicas y Desarrollo Nuclear (CEADEN), Havana, Cuba

⁸ Centro de Investigación y de Estudios Avanzados (CINVESTAV), Mexico City and Mérida, Mexico

⁹ Chicago State University, Chicago, Illinois, United States

¹⁰ China Institute of Atomic Energy, Beijing, China

¹¹ China University of Geosciences, Wuhan, China

¹² Chungbuk National University, Cheongju, Republic of Korea

¹³ Comenius University Bratislava, Faculty of Mathematics, Physics and Informatics, Bratislava, Slovak Republic

¹⁴ COMSATS University Islamabad, Islamabad, Pakistan

¹⁵ Creighton University, Omaha, Nebraska, United States

¹⁶ Department of Physics, Aligarh Muslim University, Aligarh, India

¹⁷ Department of Physics, Pusan National University, Pusan, Republic of Korea

¹⁸ Department of Physics, Sejong University, Seoul, Republic of Korea

¹⁹ Department of Physics, University of California, Berkeley, California, United States

²⁰ Department of Physics, University of Oslo, Oslo, Norway

²¹ Department of Physics and Technology, University of Bergen, Bergen, Norway

²² Dipartimento di Fisica, Università di Pavia, Pavia, Italy

²³ Dipartimento di Fisica dell'Università and Sezione INFN, Cagliari, Italy

²⁴ Dipartimento di Fisica dell'Università and Sezione INFN, Trieste, Italy

²⁵ Dipartimento di Fisica dell'Università and Sezione INFN, Turin, Italy

²⁶ Dipartimento di Fisica e Astronomia dell'Università and Sezione INFN, Bologna, Italy

²⁷ Dipartimento di Fisica e Astronomia dell'Università and Sezione INFN, Catania, Italy

²⁸ Dipartimento di Fisica e Astronomia dell'Università and Sezione INFN, Padova, Italy

²⁹ Dipartimento di Fisica 'E.R. Caianiello' dell'Università and Gruppo Collegato INFN, Salerno, Italy

³⁰ Dipartimento DISAT del Politecnico and Sezione INFN, Turin, Italy

³¹ Dipartimento di Scienze MIFT, Università di Messina, Messina, Italy

³² Dipartimento Interateneo di Fisica 'M. Merlin' and Sezione INFN, Bari, Italy

³³ European Organization for Nuclear Research (CERN), Geneva, Switzerland

³⁴ Faculty of Electrical Engineering, Mechanical Engineering and Naval Architecture, University of Split, Split, Croatia

³⁵ Faculty of Engineering and Science, Western Norway University of Applied Sciences, Bergen, Norway

- ³⁶ Faculty of Nuclear Sciences and Physical Engineering, Czech Technical University in Prague, Prague, Czech Republic
- ³⁷ Faculty of Physics, Sofia University, Sofia, Bulgaria
- ³⁸ Faculty of Science, P.J. Šafárik University, Košice, Slovak Republic
- ³⁹ Frankfurt Institute for Advanced Studies, Johann Wolfgang Goethe-Universität Frankfurt, Frankfurt, Germany
- ⁴⁰ Fudan University, Shanghai, China
- ⁴¹ Gangneung-Wonju National University, Gangneung, Republic of Korea
- ⁴² Gauhati University, Department of Physics, Guwahati, India
- ⁴³ Helmholtz-Institut für Strahlen- und Kernphysik, Rheinische Friedrich-Wilhelms-Universität Bonn, Bonn, Germany
- ⁴⁴ Helsinki Institute of Physics (HIP), Helsinki, Finland
- ⁴⁵ High Energy Physics Group, Universidad Autónoma de Puebla, Puebla, Mexico
- ⁴⁶ Horia Hulubei National Institute of Physics and Nuclear Engineering, Bucharest, Romania
- ⁴⁷ HUN-REN Wigner Research Centre for Physics, Budapest, Hungary
- ⁴⁸ Indian Institute of Technology Bombay (IIT), Mumbai, India
- ⁴⁹ Indian Institute of Technology Indore, Indore, India
- ⁵⁰ INFN, Laboratori Nazionali di Frascati, Frascati, Italy
- ⁵¹ INFN, Sezione di Bari, Bari, Italy
- ⁵² INFN, Sezione di Bologna, Bologna, Italy
- ⁵³ INFN, Sezione di Cagliari, Cagliari, Italy
- ⁵⁴ INFN, Sezione di Catania, Catania, Italy
- ⁵⁵ INFN, Sezione di Padova, Padova, Italy
- ⁵⁶ INFN, Sezione di Pavia, Pavia, Italy
- ⁵⁷ INFN, Sezione di Torino, Turin, Italy
- ⁵⁸ INFN, Sezione di Trieste, Trieste, Italy
- ⁵⁹ Inha University, Incheon, Republic of Korea
- ⁶⁰ Institute for Gravitational and Subatomic Physics (GRASP), Utrecht University/Nikhef, Utrecht, Netherlands
- ⁶¹ Institute of Experimental Physics, Slovak Academy of Sciences, Košice, Slovak Republic
- ⁶² Institute of Physics, Homi Bhabha National Institute, Bhubaneswar, India
- ⁶³ Institute of Physics of the Czech Academy of Sciences, Prague, Czech Republic
- ⁶⁴ Institute of Space Science (ISS), Bucharest, Romania
- ⁶⁵ Institut für Kernphysik, Johann Wolfgang Goethe-Universität Frankfurt, Frankfurt, Germany
- ⁶⁶ Instituto de Ciencias Nucleares, Universidad Nacional Autónoma de México, Mexico City, Mexico
- ⁶⁷ Instituto de Física, Universidade Federal do Rio Grande do Sul (UFRGS), Porto Alegre, Brazil
- ⁶⁸ Instituto de Física, Universidad Nacional Autónoma de México, Mexico City, Mexico
- ⁶⁹ iThemba LABS, National Research Foundation, Somerset West, South Africa
- ⁷⁰ Jeonbuk National University, Jeonju, Republic of Korea
- ⁷¹ Johann-Wolfgang-Goethe Universität Frankfurt Institut für Informatik, Fachbereich Informatik und Mathematik, Frankfurt, Germany
- ⁷² Korea Institute of Science and Technology Information, Daejeon, Republic of Korea
- ⁷³ KTO Karatay University, Konya, Turkey
- ⁷⁴ Laboratoire de Physique Subatomique et de Cosmologie, Université Grenoble-Alpes, CNRS-IN2P3, Grenoble, France
- ⁷⁵ Lawrence Berkeley National Laboratory, Berkeley, California, United States
- ⁷⁶ Lund University Department of Physics, Division of Particle Physics, Lund, Sweden
- ⁷⁷ Nagasaki Institute of Applied Science, Nagasaki, Japan
- ⁷⁸ Nara Women's University (NWU), Nara, Japan
- ⁷⁹ National and Kapodistrian University of Athens, School of Science, Department of Physics, Athens, Greece
- ⁸⁰ National Centre for Nuclear Research, Warsaw, Poland
- ⁸¹ National Institute of Science Education and Research, Homi Bhabha National Institute, Jatni, India
- ⁸² National Nuclear Research Center, Baku, Azerbaijan
- ⁸³ National Research and Innovation Agency - BRIN, Jakarta, Indonesia
- ⁸⁴ Niels Bohr Institute, University of Copenhagen, Copenhagen, Denmark
- ⁸⁵ Nikhef, National institute for subatomic physics, Amsterdam, Netherlands
- ⁸⁶ Nuclear Physics Group, STFC Daresbury Laboratory, Daresbury, United Kingdom
- ⁸⁷ Nuclear Physics Institute of the Czech Academy of Sciences, Husinec-Řež, Czech Republic

- 88 Oak Ridge National Laboratory, Oak Ridge, Tennessee, United States
- 89 Ohio State University, Columbus, Ohio, United States
- 90 Physics department, Faculty of science, University of Zagreb, Zagreb, Croatia
- 91 Physics Department, Panjab University, Chandigarh, India
- 92 Physics Department, University of Jammu, Jammu, India
- 93 Physics Program and International Institute for Sustainability with Knotted Chiral Meta Matter (SKCM2), Hiroshima University, Hiroshima, Japan
- 94 Physikalisches Institut, Eberhard-Karls-Universität Tübingen, Tübingen, Germany
- 95 Physikalisches Institut, Ruprecht-Karls-Universität Heidelberg, Heidelberg, Germany
- 96 Physik Department, Technische Universität München, Munich, Germany
- 97 Politecnico di Bari and Sezione INFN, Bari, Italy
- 98 Research Division and ExtreMe Matter Institute EMMI, GSI Helmholtzzentrum für Schwerionenforschung GmbH, Darmstadt, Germany
- 99 Saga University, Saga, Japan
- 100 Saha Institute of Nuclear Physics, Homi Bhabha National Institute, Kolkata, India
- 101 School of Physics and Astronomy, University of Birmingham, Birmingham, United Kingdom
- 102 Sección Física, Departamento de Ciencias, Pontificia Universidad Católica del Perú, Lima, Peru
- 103 Stefan Meyer Institut für Subatomare Physik (SMI), Vienna, Austria
- 104 SUBATECH, IMT Atlantique, Nantes Université, CNRS-IN2P3, Nantes, France
- 105 Sungkyunkwan University, Suwon City, Republic of Korea
- 106 Suranaree University of Technology, Nakhon Ratchasima, Thailand
- 107 Technical University of Košice, Košice, Slovak Republic
- 108 The Henryk Niewodniczanski Institute of Nuclear Physics, Polish Academy of Sciences, Cracow, Poland
- 109 The University of Texas at Austin, Austin, Texas, United States
- 110 Universidad Autónoma de Sinaloa, Culiacán, Mexico
- 111 Universidade de São Paulo (USP), São Paulo, Brazil
- 112 Universidade Estadual de Campinas (UNICAMP), Campinas, Brazil
- 113 Universidade Federal do ABC, Santo Andre, Brazil
- 114 Universitatea Nationala de Stiinta si Tehnologie Politehnica Bucuresti, Bucharest, Romania
- 115 University of Cape Town, Cape Town, South Africa
- 116 University of Derby, Derby, United Kingdom
- 117 University of Houston, Houston, Texas, United States
- 118 University of Jyväskylä, Jyväskylä, Finland
- 119 University of Kansas, Lawrence, Kansas, United States
- 120 University of Liverpool, Liverpool, United Kingdom
- 121 University of Science and Technology of China, Hefei, China
- 122 University of South-Eastern Norway, Kongsberg, Norway
- 123 University of Tennessee, Knoxville, Tennessee, United States
- 124 University of the Witwatersrand, Johannesburg, South Africa
- 125 University of Tokyo, Tokyo, Japan
- 126 University of Tsukuba, Tsukuba, Japan
- 127 Universität Münster, Institut für Kernphysik, Münster, Germany
- 128 Université Clermont Auvergne, CNRS/IN2P3, LPC, Clermont-Ferrand, France
- 129 Université de Lyon, CNRS/IN2P3, Institut de Physique des 2 Infinis de Lyon, Lyon, France
- 130 Université de Strasbourg, CNRS, IPHC UMR 7178, F-67000 Strasbourg, France, Strasbourg, France
- 131 Université Paris-Saclay, Centre d’Etudes de Saclay (CEA), IRFU, Département de Physique Nucléaire (DPHN), Saclay, France
- 132 Université Paris-Saclay, CNRS/IN2P3, IJCLab, Orsay, France
- 133 Università degli Studi di Foggia, Foggia, Italy
- 134 Università del Piemonte Orientale, Vercelli, Italy
- 135 Università di Brescia, Brescia, Italy
- 136 Variable Energy Cyclotron Centre, Homi Bhabha National Institute, Kolkata, India
- 137 Warsaw University of Technology, Warsaw, Poland
- 138 Wayne State University, Detroit, Michigan, United States
- 139 Yale University, New Haven, Connecticut, United States
- 140 Yonsei University, Seoul, Republic of Korea

¹⁴¹ Zentrum für Technologie und Transfer (ZTT), Worms, Germany

¹⁴² Affiliated with an institute covered by a cooperation agreement with CERN

¹⁴³ Affiliated with an international laboratory covered by a cooperation agreement with CERN.